SANDIA REPORT

SAND90–2104 • UC–920
Unlimited Release
Printed September 1996

Characterization of MgO Powders for Use in Thermal Batteries

Ronald A. Guidotti, Frederick W. Reinhardt

Prepared by
Sandia National Laboratories
Albuquerque, New Mexico 87185 and Livermore, California 94550
for the United States Department of Energy
under Contract DE-AC04-94AL85000

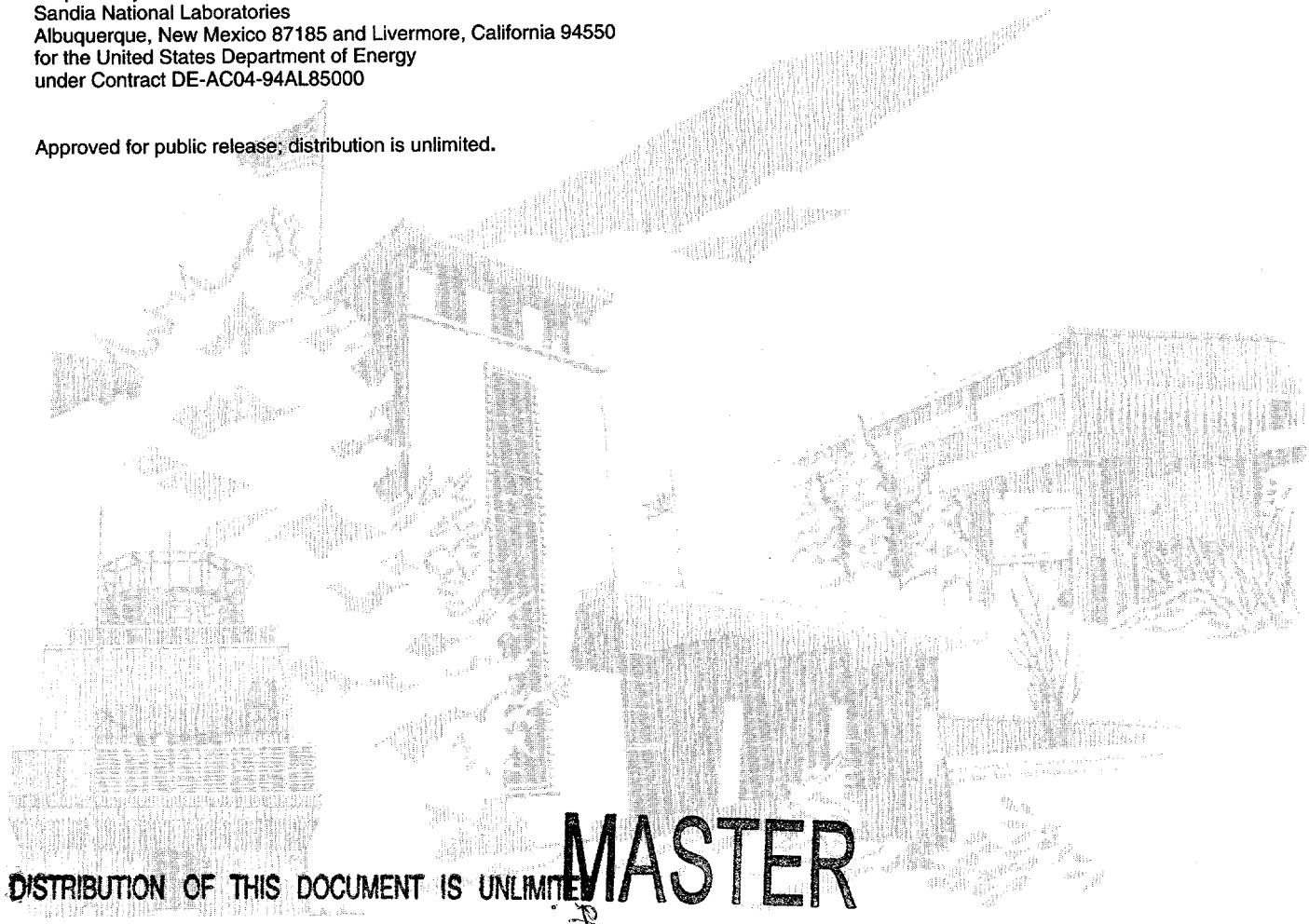

Issued by Sandia National Laboratories, operated for the United States Department of Energy by Sandia Corporation.

Available to DOE and DOE contractors from
Office of Scientific and Technical Information
PO Box 62
Oak Ridge, TN 37831

Prices available from (615) 576-8401, FTS 626-8401

Available to the public from
National Technical Information Service
US Department of Commerce
5285 Port Royal Rd
Springfield, VA 22161

NTIS price codes
Printed copy: A03
Microfiche copy: A01

SAND90-2104
Unlimited Release
Printed September 1996

Distribution
Category UC-920

Characterization of MgO Powders for Use in Thermal Batteries

Ronald A. Guidotti and Frederick W. Reinhardt

Battery Research Department
Sandia National Laboratories
Albuquerque, NM 87185-5800

Abstract

Ten commercial MgO powders were evaluated for their suitability to act as a binder in the separator of thermal batteries to immobilize the electrolyte when it is molten. One brand in particular, Maglite S from Calgon, outperformed all the others. This report describes the results of a characterization study of this MgO as well as similar materials from other commercial vendors. The study objective was to define the critical properties of Maglite S MgO that are responsible for its superior performance in thermal-battery separators. Separator mixes were prepared with the various MgO powders and the resulting powders and pellets were characterized, to correlate key physical properties of these materials to select physical and chemical properties of the MgO powders used in their preparation. The MgO pore-size distribution was the only parameter that could be related to the deformation and electrolyte-leakage behavior of separator pellets. A potential replacement for the Maglite S is currently being qualified, since Maglite S MgO is no longer available.

Acknowledgments

The authors wish to acknowledge the assistance of the following persons. B. Mckenzie, 1822, for the scanning electron photomicrographs and R. W. Bild and B. Campbell-Domme, formerly of 1846, for the neutron activation and emission spectrographic analyses. Dr. Douglas Smith, of the Department of Chemical and Nuclear Engineering at the University of New Mexico performed the nuclear-magnetic-resonance (NMR) experiments.

Contents

Figures

Tables

Characterization of MgO Powders for Use in Thermal Batteries

Introduction

The separator in Li-alloy/FeS_2 thermal batteries uses MgO powder to immobilize the molten-salt phase by capillary action during operation. Typically, LiCl-KCl eutectic, which melts at 352°C, is used for many battery applications. Operating temperatures usually range from 400 °C to 550 °C. Thermal batteries designed at Sandia National Laboratories/New Mexico use a MgO designated as Maglite S (#3331), manufactured by Calgon (Pittsburgh, PA). In earlier work by Searcy *et al.*, this material was found to possesses unique properties that made it the best suited of the commercially available MgO powders examined at that time for this application.[1]

When used in separator mixes–also called electrolyte-binder (EB) mixes–with LiCl-KCl eutectic, a minimum of ~35% Maglite S MgO is necessary to adequately immobilize the molten electrolyte for most applications. Under more severe conditions (*e.g.*, high shock and vibration), the binder content must be increased somewhat–typically, to 40%. (Unless otherwise noted, all compositions are reported as weight percentage.) With other electrolytes, the minimum amount of Maglite S MgO required for adequate immobilization can be the same or even less.[2]

The adequacy of immobilization is determined by the deformation of EB pellets at 530°C under an applied pressure.[3,4] It has been determined empirically that a nominal deformation (reduction in thickness) of 15% to 30% is ideal. This amount of EB deformation is necessary to allow good interfacial contact with the anode and cathode pellets.[3] The benefits of this are minimum voltage losses during discharge (*i.e.*, it results in a lower battery impedance). Deformation greater than this range results in excessive extrusion with concomitant electrolyte leakage into the insulating wrap surrounding the battery stack. This leads to high parasitic current losses that adversely impact battery performance.

When EB mixes are made with MgO powders other than Maglite S, the extent of deformation that is observed is unacceptably high.[1] A study was therefore undertaken to identify parameters that are responsible for the unique properties of Maglite S MgO that make it so ideally suited for thermal-batteries. The primary objective was to correlate the chemical and physical properties of the various MgO powders with their effectiveness for immobilization of molten electrolyte.

In the present study, only EBs made with LiCl-KCl eutectic were evaluated. In all, 11 commercial sources of MgO were examined, although not all were studied to the same degree. Parameters that were measured for the MgO included: chemical composition (impurities), BET surface area, particle-size distribution, and pore-size distribution. The resulting EB mixes were also characterized for possible correlation of their physical properties to those of the MgO materials. Properties measured included: BET surface area, particle-size distribution, flow properties, and pore-size distribution. In addition, nuclear magnetic resonance (NMR) spin-lattice relaxation measurements were

made with both the MgO powders and the corresponding EB powders using *n*-heptane as the sorbate.

Experimental Procedures

Materials

The MgO powders that were examined are listed in Table 1. Near the end of the study, it was discovered that Maglite S would no longer be produced. This added a sense of urgency to the study, in that a suitable replacement would now have to be found and qualified. The manufacturer of Maglite S recommended Marinco OL (Marine Magnesium Co., Coraopolis, PA) as a possible replacement and it was added to the study. It is still undergoing evaluation tests and has not been fully qualified at this time.

TABLE 1. Sources of MgO Examined in the Characterization Study

MgO Source	MgO Type
Baker	N.A.
Calgon	Maglite A
Calgon	Maglite S
Combustion Engineering	MAGOX 90HR -325
Combustion Engineering	MAGOX 98HR Fine
Mallinckrodt	N.A.
Marine Magnesium Co.	Marinco OL
Martin-Marietta	N.A.
Meller	N.A.
Morton	90
Morton	170

N.A. = not applicable.

Processing

All processing of MgO, electrolyte, and EBs was conducted in a dry room maintained at <1% relative humidity (<300 ppm moisture). Most of the characterization tests–flow properties, electrolyte leakage, and pellet deformation–were also done in the dry room, as was sample preparation for measurement of particle-size and pore-size distributions.

EB Preparation. Before use, the MgO powders were baked at 600 °C for four hours in quartz trays to remove any hydroxide and carbonate impurities. The eutectic electrolyte was prepared by fusing the appropriate amounts of LiCl (45%) and KCl (55%) in a quartz crucible at 650 °C for four hours. The melt was then quenched in an Inconel tray and granulated in a hammer mill to a fine powder of 10-20 micrometers.

The EB mixes were prepared by mixing the calcined MgO powders with the required amount of LiCl-KCl eutectic electrolyte using liquid Freon TF in a blender.[5] An EB composition of 35% MgO and 65% electrolyte was used for most of the samples.

The EB slurry was then placed into a convection oven to remove the Freon and the resulting "cake" was then fused at 400°C for 16 hours in the dry room. After cooling, the fused cake was then granulated and then passed through a U.S. Standard 60-mesh screen.

Measurement Techniques

Impurities. The metallic impurity levels in the MgO powders were measured using 14-MeV neutron activation analysis (NAA) and atomic emission spectroscopy (AES). Non-metallic (anionic) impurities were determined by ion chromatography.

BET Surface Area. The BET surface areas of the MgO and EB powders were measured using a Micromeritics Model 2100 BET analyzer (Norcross, GA) or a Quantachrome Monosorb Surface Area Analyzer (Syossett, NY).

Particle-Size Distribution. The particle-size distributions of the MgO and EB powders were determined using a Sedigraph 5000 (Micromeritics, Norcross, GA) and Sedisperse P-11 as the medium.

Flow Properties. The flow properties of the EB powders were determined using the angle-of-repose technique. A pedestal 2.54 cm in diameter was used to support the powder. The powder was fed through a vibrating screen and allowed to fall on the pedestal. The height of the cone on the pedestal was then measured to calculated the angle of repose.[6] These measurements were made in triplicate and then averaged.

Pore-Size Distribution. The pore-size distributions of the MgOs and the EBs were determined by mercury porosimetry at Micromeritics using their Model Auto-Pore 9200. Care was taken when using EB samples to minimize exposure to ambient moisture when loading the samples. Generally, the EB samples used were pellets.

Deformation. The effectiveness of electrolyte immobilization was determined by measurement of the deformation properties of EB pellets and their tendency for electrolyte leakage when molten.

The deformation of the EB pellets was determined by measuring the reduction in thickness at 530°C under an applied pressure of 99 kPa (14.3 psig). This procedure is identical to that previously described for catholyte pellets for $Ca/CaCrO_4$ thermal batteries.[6] The EB pellets for this test were 3.18 cm in diameter and 0.153 cm thick. The change in thickness of the pellet was virtually instantaneous once melting occurred and changed little with time up to over five minutes.[3] However, for this study, the reduction in thickness after three minutes at temperature was taken as the deformation. The reported deformation data are the average of three separate samples.

Electrolyte Leakage. The tendency for electrolyte leakage was determined using EB pellets and the technique developed earlier for catholyte pellets for $Ca/CaCrO_4$ thermal batteries.[6]

Basically, the leakage tests consisted of immersing a weighed EB pellet in a bed of alumina in a 50-cc Pyrex beaker; the alumina used was gas-chromatographic grade (Fisher A-504, Fair Lawn, NJ).[4] An array of beakers was loaded in a stainless steel tray along with a thermocoupled control beaker containing only the alumina. The sample tray was then placed in an oven at 400°C and allowed to heat to temperature.

After 30 minutes at temperature, the sample tray was removed and the samples allowed to cool to ambient. The pellets were then removed from the beakers, brushed free of alumina and salt, and reweighed. The mass loss was then normalized to a mass loss per unit area for relative comparison. The reported leakage data are the average of three separate samples.

Differential Scanning Calorimetry. Differential scanning calorimetry (DSC) was used to measure the melting points of the various EB mixes, since impurities can result in lowering of the liquidus. The samples were loaded in gold pans in the glovebox under high-purity argon. A Perkin-Elmer

DSC-2 was used for all the DSC measurements.

Spin-Lattice Relaxation Tests. NMR spin-lattice relaxation measurements can provide valuable information regarding the pore structure of materials.[7-9] The measurements were conducted at 30°C and 20 MHz using a Spin-Lock GPS-2 pulse NMR. A 180°-τ-90° RF pulse sequence was used and the height of the free induction decay was obtained as a 180°-τ-90° RF pulse sequence. The height of the free induction decay was obtained as a function of τ (time between pulses) using a Nicolet 2090 digital oscilloscope interfaced to an IBM CS-9000 computer. The observed magnetization, M(τ), was related to the distribution of spin-lattice decay times using a non-negative least-squares fit.

The typical adsorbate used for these tests is generally water, since it provides a strong hydrogen signal. However, water could not be used with the MgO powders, since it reacts to form $Mg(OH)_2$. *n*-Hexane was examined as the first alternative but was incompatible. When allowed to equilibrate with the *n*-hexane vapors, the MgO would turn purple in color. This was unexpected and suggests that there was some interaction of the MgO or impurities therein with the *n*-hexane to form a colored complex. The second adsorbate tried was *n*-heptane; no colored complexes were observed with this material.

A typical run consisted of pumping out the sample in a special holder to 10 millitorr for at least an hour. The *n*-heptane was allowed to equilibrate overnight at ambient temperature with the MgO or EB sample that was then analyzed by NMR. The same procedures were used for the EB mixes, except that the necessary operations were conducted in a glove box to avoid exposure of the samples to the ambient atmosphere.

Processing Effects

Wetting. The interaction of the MgO powders and the molten electrolyte is strongly influenced by the wetting characteristics of the solid MgO and the surrounding atmosphere. This is illustrated schematically in Figure 1 where a solid block of material is shown in contact with a liquid phase. The contact angle of the liquid is defined by the tangent of the line to the surface of the liquid where it contacts the solid. A low contact angle is indicative of good wetting, whereas a high contact angle represents poor wetting. Angles less than 90° are generally considered to be wetting and angles higher than that are considered to be non-wetting. α-Bromonaphthalene, for example, has a contact angle of 5° on a soda-lime glass surface; this indicates extremely good wetting. Mercury, however, does not wet glass under the same conditions and exhibits a contact angle of 140°.[10]

The relative surface tensions of the three interfaces ultimately determines the contact angle that results.[11,12] The solid-vapor surface tension, γ_{SV}, reflects the interaction of the gaseous phase with the solid phase. The liquid-solid surface tension, γ_{LS}, reflects the interation of the liquid phase with the solid phase. The liquid-vapor surface tension, γ_{LV}, reflects the interaction of the gaseous phase with the liquid phase. The net interaction is defined mathematically by Young's equation:

$$\gamma_{LV}\cos(\Theta) = \gamma_{SV} - \gamma_{SL} \qquad [1]$$

In the case of the interaction of the molten salts with the MgO, the factors that are

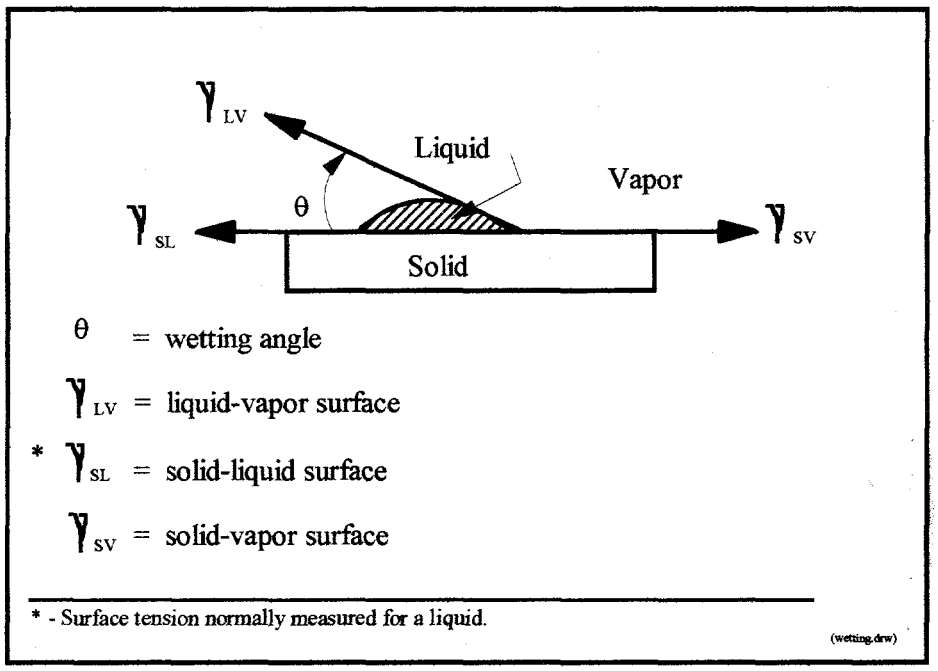

FIGURE 1. Schematic Representation of Wetting of Solid by Liquid Phase

relevant are:

- composition of the MgO (i.e., impurities)
- composition of the molten salt
- composition of the atmosphere
- surface tension of the molten salt
- temperature

The first factor affects the γ_{SV} and γ_{SL} terms in eqn. 1; the second factor affects the γ_{LV} term in eqn. 1; and the third factor affects the γ_{SV} and γ_{LV} terms in eqn. 1. The surface tension (fourth factor) and viscosity of the molten salt are dependent upon temperature (fifth factor), typically being less at the higher temperatures.

Normally, the EB mixes made with LiCl-KCl eutectic are fused in an atmosphere of dry-room air at 400°C. A good example of the significance that atmosphere can have on wetting is illustrated in an earlier experiment with an EB mix based on a SiO_2 binder. When the mixture of electrolyte and binder was fused at 400°C under high-purity argon in a glovebox, very little wetting of the SiO_2 was observed. It was necessary to increase the fusion temperature to 500°C to obtain the equivalent wetting that resulted at 400°C under dry-room conditions. This is an example of a dramatic effect that atmosphere can have upon the interaction of molten salt and binder.

Processing parameters that affect the wetting process during fusion of EB mixes are temperature, time, and packing. The temperature and time parameters are interrelated; i.e., for a given temperature and time, equivalent results can be obtained at higher temperatures for shorter times or lower temperatures for longer times. The packing of salt and MgO particles determines the relative particle-particle interaction that will initially occur before melting of the salt. This, in turn, will depend upon the relative particle-size distribution of the MgO and

electrolyte and the morphology (aspect ratio) of the particles.

Results

MgO Properties

MgO Purity. The levels of impurities as measured by NAA are listed in Table A-1 in Appendix A for the various MgO powders. The powders are ranked in order of decreasing effectiveness for immobilization of molten salt in separator pellets. The ranking results from the pellet-deformation test, which was found to be a good metric for this process.

Values listed with asterisks are valid for *relative* comparisons among the various samples. Since individual standards were not available for these elements at the time of analysis, absolute values cannot be assigned. Supplemental data from AES are listed in Table A-2 in Appendix A. The precision of the AES data can vary by a factor of two or more. Consequently, AES isn't as sensitive as NAA for some elements. Still, the relative trends can still be examined for comparison.

The major impurities in generally decreasing concentrations in the MgO powders were Ca, Si, Fe, B, Mn, Cr, and Na. The Morton 170 MgO had the highest level of metallic impurities and the Meller MgO had the lowest. However, there was no obvious association of the levels of the listed impurities with the effectiveness of the MgO as a binder in separator mixes. The impurities in the Maglite S MgO and their associated levels were not unique to this material, which was the best suited for use as a binder in the separator layer.

Several non-metallic impurities were examined for two of the MgO powders. The Maglite S, which is an excellent binder for molten salts, was used as a reference material. The Mallinckrodt MgO, which has poor binder qualities, was chosen for relative comparison. The samples were analyzed for halides, nitrate, and sulfate. In addition, the carbon and hydrogen contents were measured as indicators for the presence of carbonate and hydroxide, respectively, since these could not be readily determined directly. The results are summarized in Table 2. There was no correlation of concentration of non-metallic impurities with the efficiency of the MgO for electrolyte immobilization.

Surface Area. The surface areas of the MgO powders are listed in Table 3 along with the corresponding deformation data for

TABLE 2. Results of Analysis for Non-Metallic Impurities in Two MgO Samples

MgO Source	% Cl	% Br	%F	% SO_4	% NO_3	% C	% H
Maglite S	0.083	0.001	0.013	0.059	0.030	0.07	0.11
Mallinckrodt	0.096	0.001	0.010	0.039	0.031	0.04	0.04

TABLE 3. Deformation of EB Pellets and Surface Areas of MgO Powders Used in Their Preparation

MgO Source	% Reduction in Thickness	BET Surface Area, m^2/g
Maglite S	21.0 ± 0.9	30.6
Morton 90	37.2 ± 10.5	71.7
Maglite A	46.1 ± 9.9	18.8
Baker	54.7 ± 1.6	76.9
Morton 170	57.7 ± 3.0	50.4
Mallinckrodt	65.6 ± 0.8	23.3
Martin-Marietta	81.8 ± 4.5	23.3
Meller	93.0 ± 1.4	47.6
MAGOX 90HR -325	N.D.	N.D.
MAGOX 98HR Fine	N.D.	68*

N.D. = not determined (see text).
* Manufacturer's data.

the EB pellets. The data are ranked in decreasing order of effectiveness for immobilization of molten electrolyte. As was noted for the impurities, there was no correlation of the surface areas of the MgO powders with their ranking for electrolyte immobilization. Meller MgO, for example, ranked the lowest, yet its surface area was similar to that for Morton 170 MgO which had a much lower deformation.

It should be noted that the deformation of 37.2% noted with Morton 90 is slightly above the upper value of ~30% empirically determined to be acceptable. This material was marginally acceptable. The deformation observed for the other MgO powders, however, would be totally unacceptable at this binder level.

No deformation data are listed for the two MAGOX MgO powders from Combustion Engineering because it was not possible to prepare EB mixes with these materials. During the fusion of the EB mixes, the molten salt separated from the MgO powders and collected in the bottom of the quartz trays. Because of their unacceptable characteristics for functioning as a binder for molten-salts, these materials were dropped from the characterization study.

MgO Particle-Size Distribution. The particle-size distributions of the various MgO powders are summarized in Figure 2. Data were not available for the Morton 90 and the Mallinckrodt MgO powders. The median particle sizes are listed in Table 4. The Morton 170 MgO had the smallest median particle size while the Meller MgO had the largest. Materials with the larger particle sizes didn't hold the electrolyte as well and performed poorly as binders.

The Maglite S MgO differed from the other MgO powders, however, in that it showed a

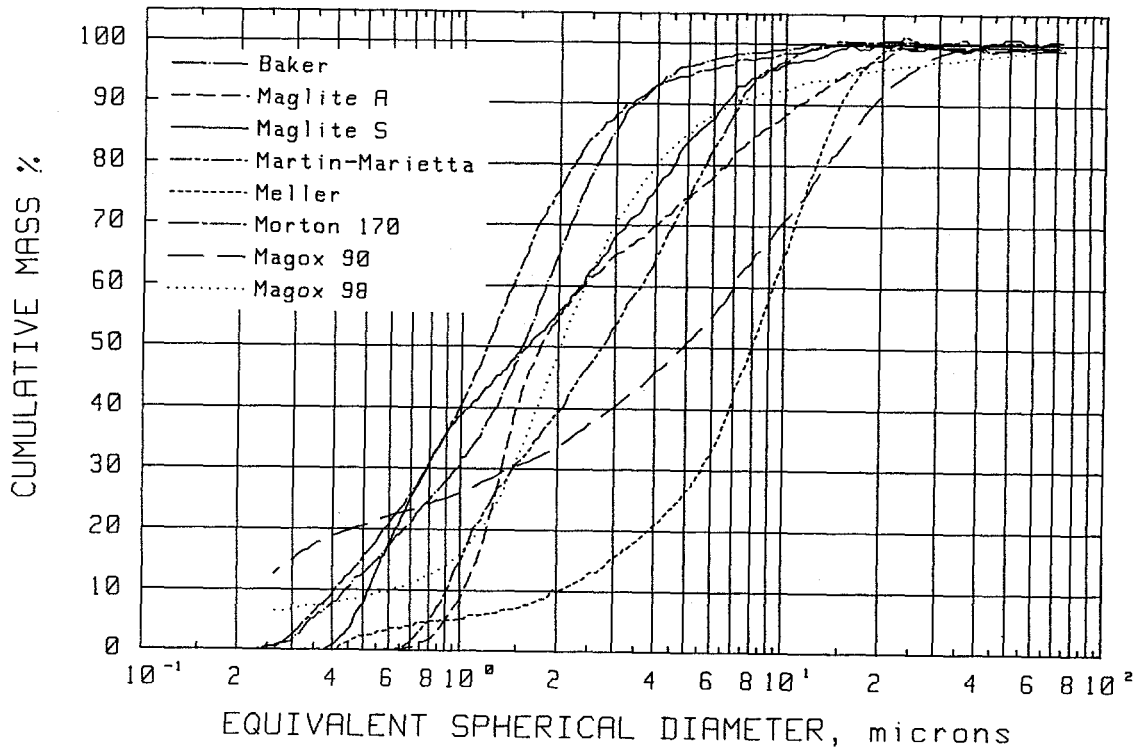

FIGURE 2. Particle-Size Distribution of MgO Powders After Calcining At 600°C/4 Hours

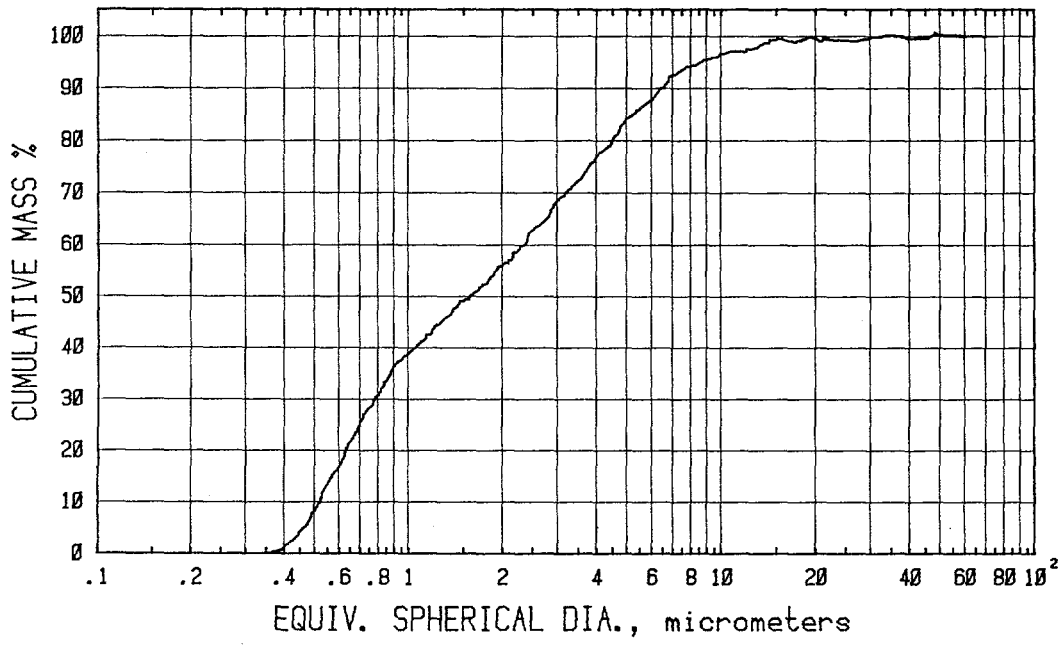

FIGURE 3. Particle-Size Distribution of Maglite S MgO After Calcining At 600°C/4 Hours

TABLE 4. Median Particle Sizes of MgO Powders as Determined by Sedigraph

MgO Source	Median Particle Size, μm
Maglite S	1.61
Morton 90	N.A.
Maglite A	1.75
Baker	1.54
Morton 170	1.20
Mallinckrodt	N.A.
Martin-Marietta	2.74
Meller	8.04
MAGOX 90HR	4.86
MAGOX 98HR	2.02

bimodal distribution. This is more readily evident in Figure 3.

Sample Morphology. SEM photomicrographs of the various MgO powders were taken to document the morphology of these materials. The results for materials calcined at 600°C for four hours are summarized in Figures 4-13. (The sizes of the particles can be estimated from the markers on the photomicrographs.)

The morphologies varied considerably. The Maglite S had a fluffy, slightly fibrous open structure (Figure 4). The Baker and Meller MgO powders had platelet structures (Figures 7 and 11, respectively). The Maglite A and Martin-Marietta MgO powders, on the other hand, contained loosely bound, rounded agglomerates (Figures 6 and 10, respectively). Both of the MgO powders from Combustion Engineering and that from Meller (Figures 12, 13, and 11, respectively) showed dense sintered particles. The rather coarse sintered structure is in agreement with the large median particle sizes as determined by sedimentation. The lack of significant porosity is consistent with their poor performance as binders for molten salts.

Care should be taken, however, when comparing the SEM photomicrographs and the particle-size distribution data. The presence of agglomerates visible in the SEM photomicrographs may not necessarily correlate to large particles as determined by the sedimentation technique. As part of the preparation for analysis, the MgO powders are ultrasonically agitated for 10 minutes before the sedimentation analysis by the Sedigraph. Consequently, some of the agglomerates could be broken down into smaller particles that would result in a lower median particle size than might be observed from the corresponding SEM photomicrographs.

Pore-Size Distribution. The pore-size distributions of the various MgO powders are summarized in Figure 14 on a volume basis and on a relative-distribution basis in Figure 15. The median pore sizes are listed in Table 5 and ranged from 0.65 μm to 3.71 μm.

Interpretation of the mercury-porosimetry data is complicated by the need to separate interparticle filling of mercury from intraparticle filling.[13,14] Generally, the former takes place at much lower pressures. This could result in the plateaux evident in the distribution curves.

Examination of the data for Figure 15 for Maglite S MgO shows that it had a lower percentage of fine pores. Maglite A MgO had a similar pore distribution in this region. However, the EB made with 35% Maglite A

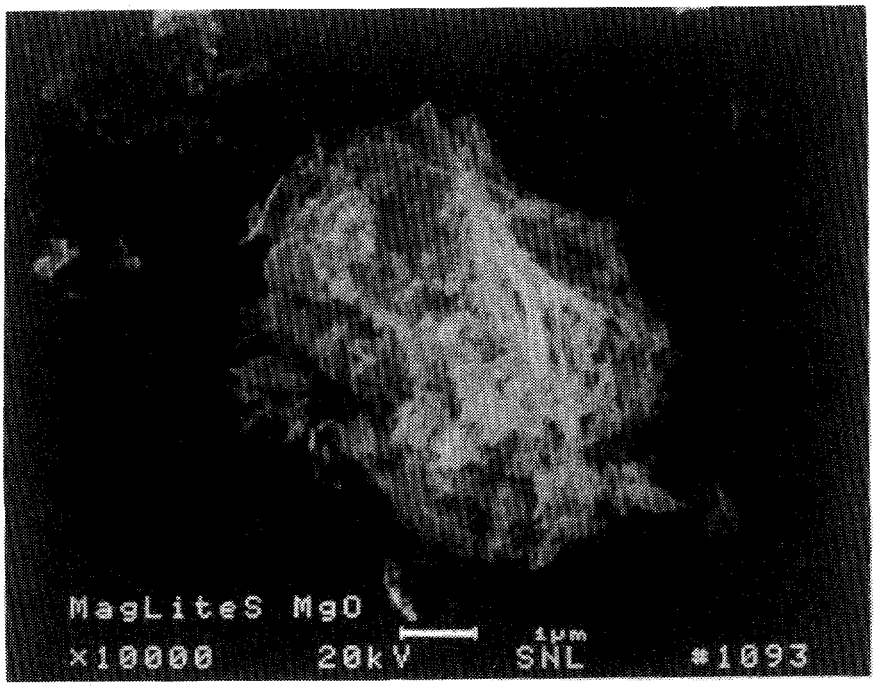

FIGURE 4. SEM Photomicrograph of Maglite S MgO After Calcining at 600°C/4 Hours

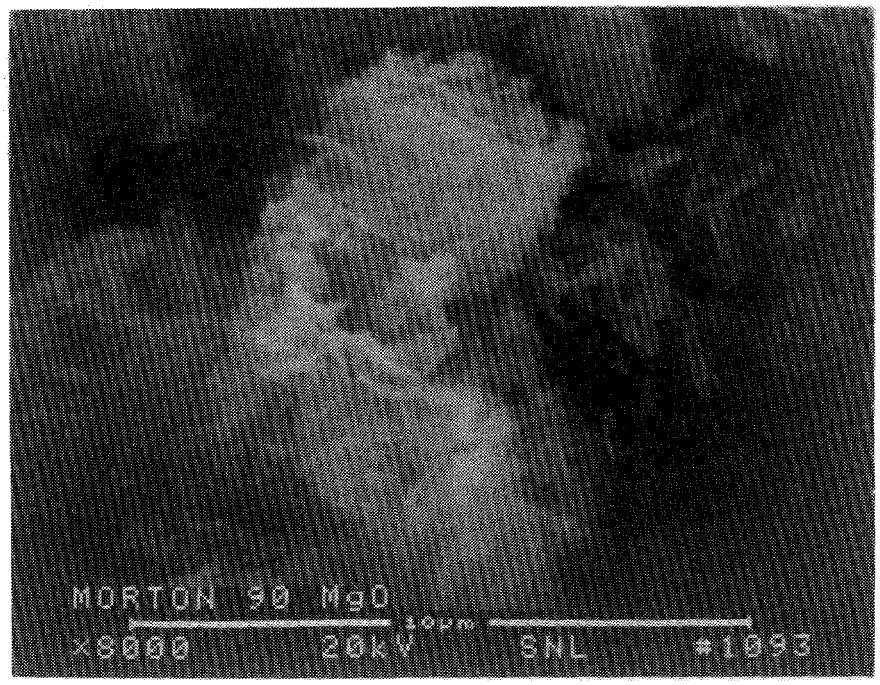

FIGURE 5. SEM Photomicrograph of Morton 90 MgO After Calcining at 600°C/4 Hours

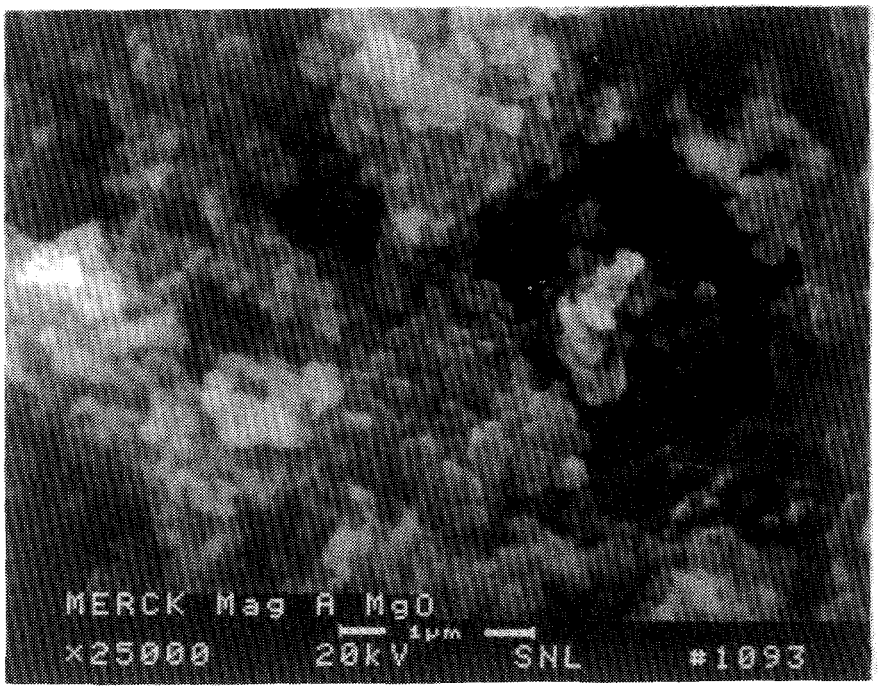

FIGURE 6. SEM Photomicrograph of Maglite A MgO After Calcining at 600°C/4 Hours

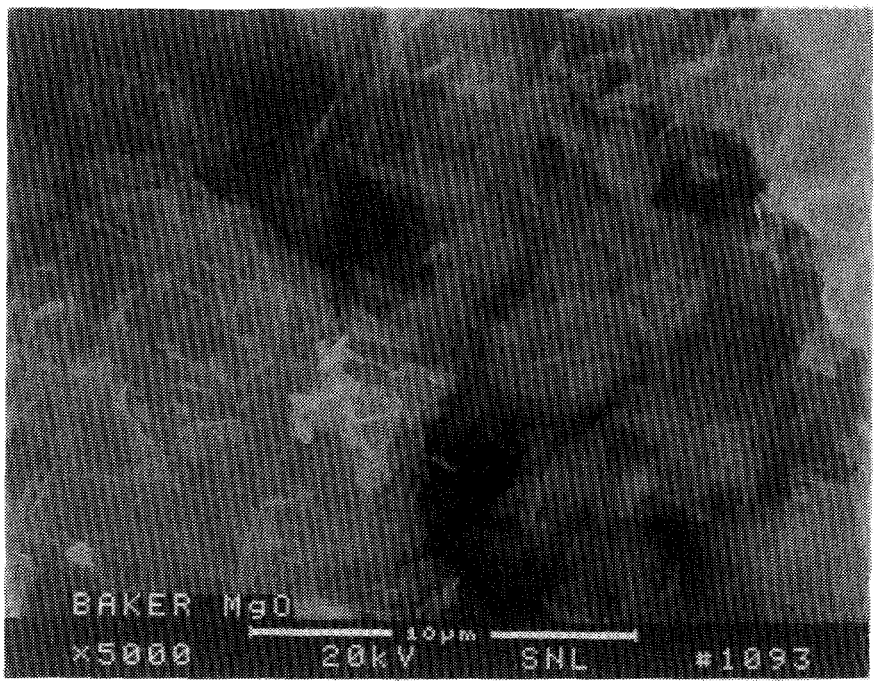

FIGURE 7. SEM Photomicrograph of Baker MgO After Calcining at 600°C/4 Hours

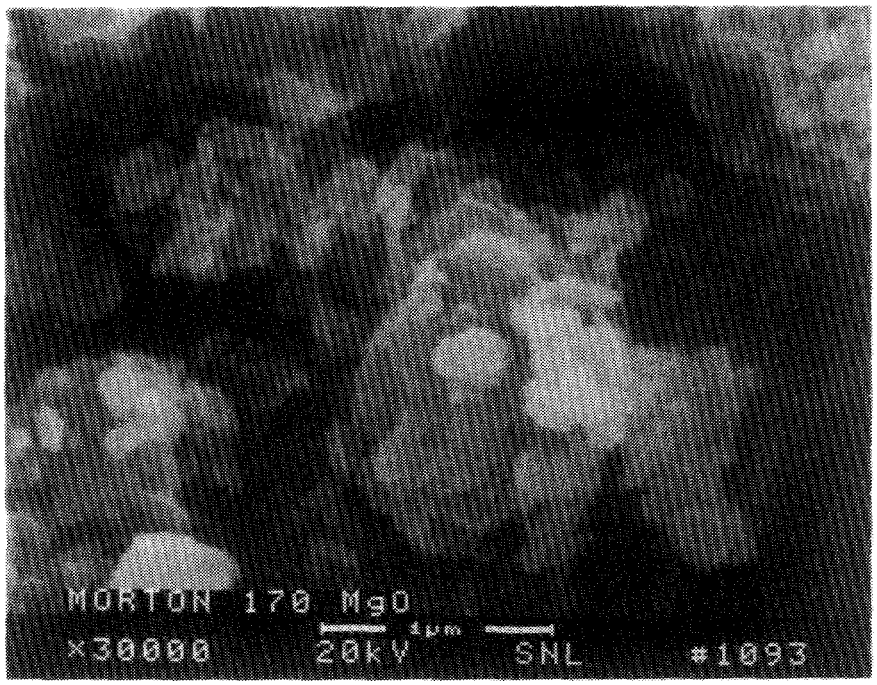

FIGURE 8. SEM Photomicrograph of Morton 170 MgO After Calcining at 600°C/4 Hours

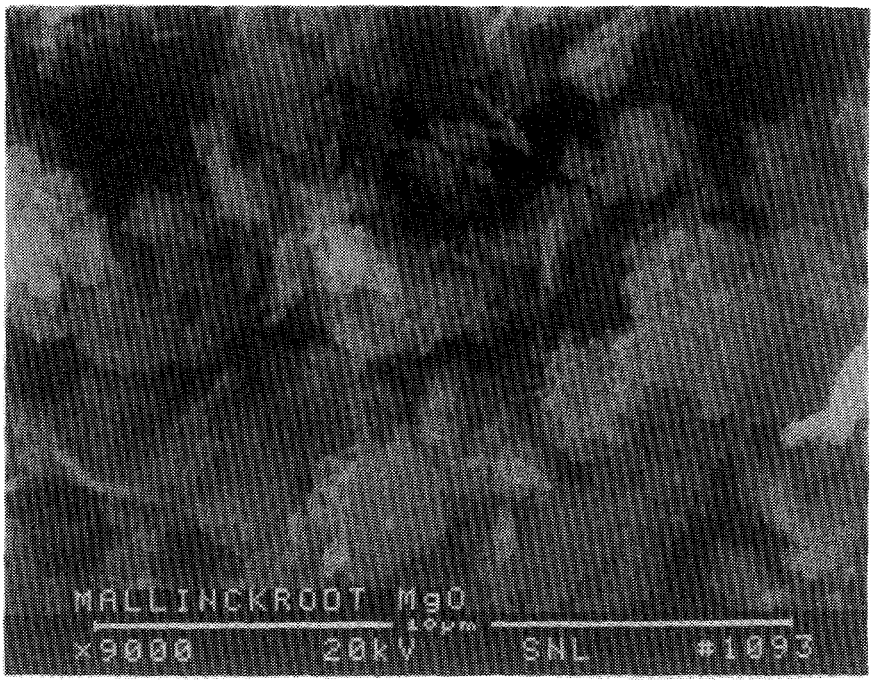

FIGURE 9. SEM Photomicrograph of Mallinckrodt MgO After Calcining at 600°C/4 Hours

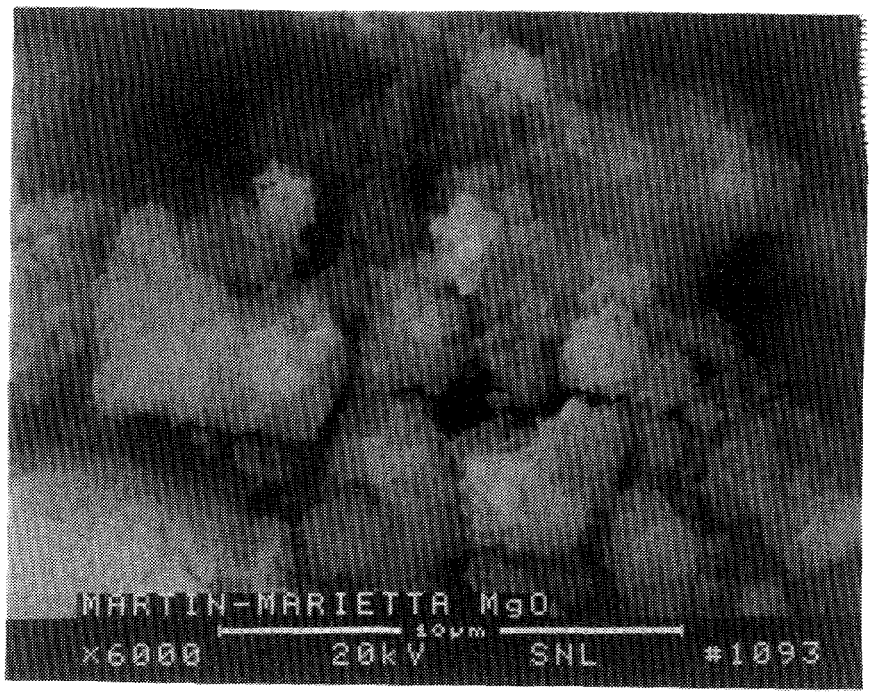

FIGURE 10. SEM Photomicrograph of Martin-Marietta MgO After Calcining at 600°C/4 Hours

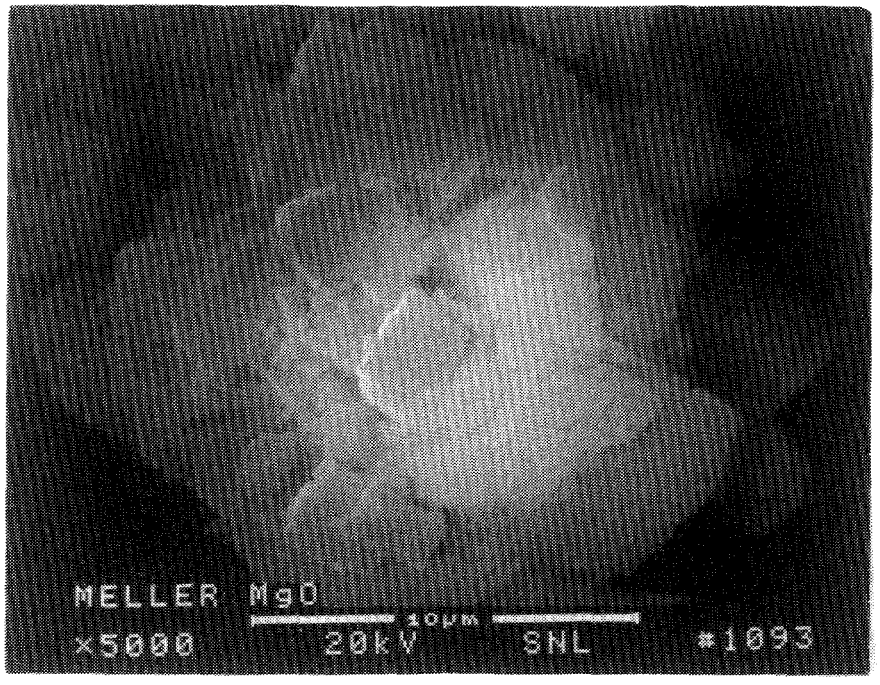

FIGURE 11. SEM Photomicrograph of Meller MgO After Calcining at 600°C/4 Hours

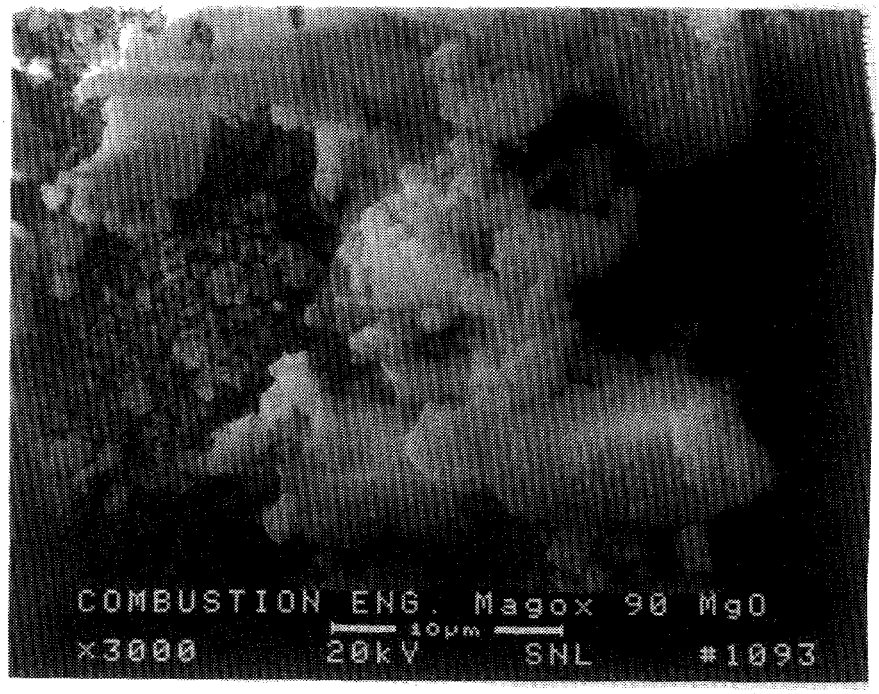

FIGURE 12. SEM Photomicrograph of MAGOX 90 MgO After Calcining at 600°C/4 Hours

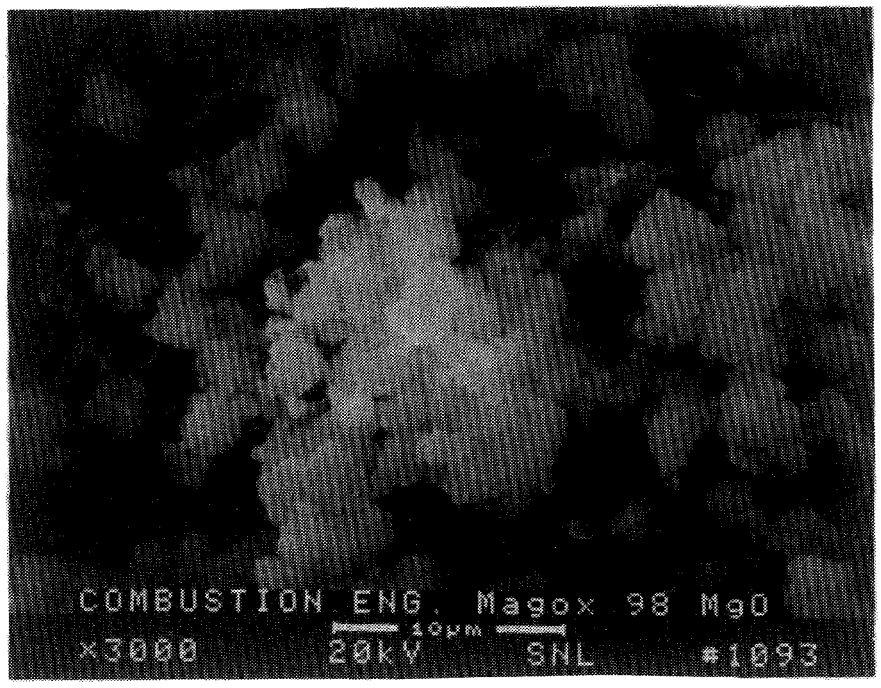

FIGURE 13. SEM Photomicrograph of MAGOX 98 MgO After Calcining at 600°C/4 Hours

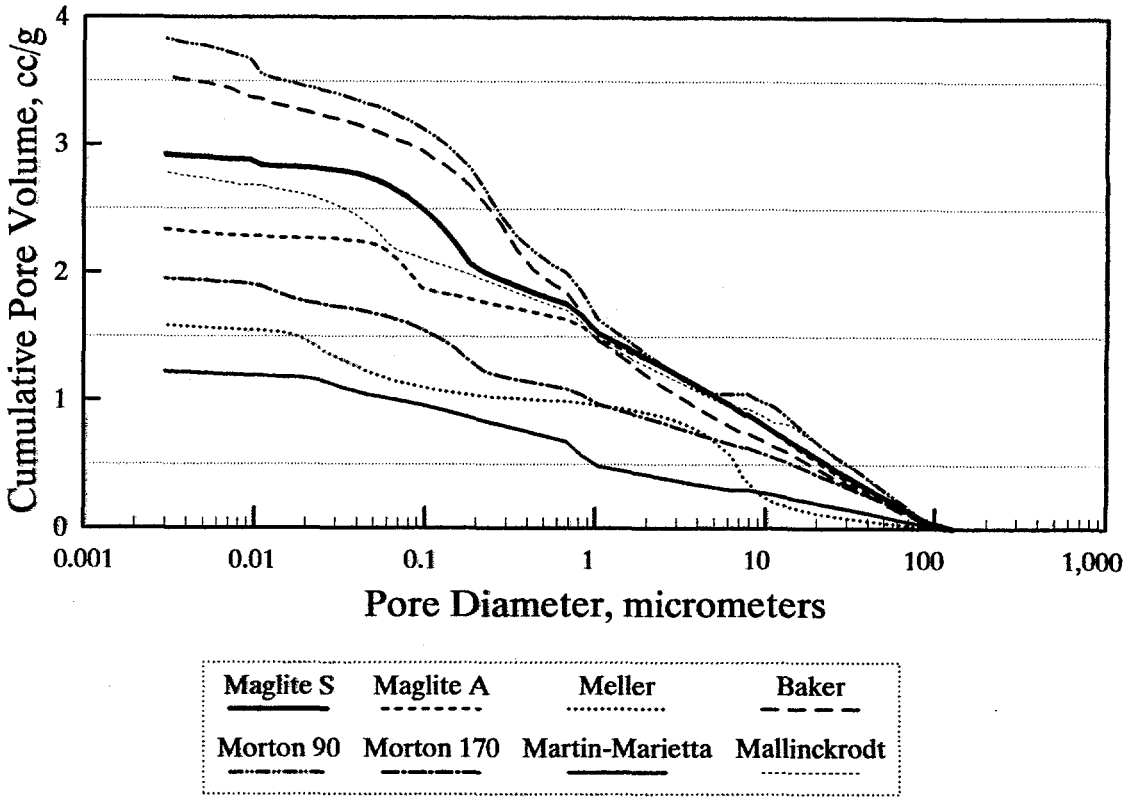

FIGURE 14. Pore-Size Distribution of MgO Powders on Volume Basis After Calcining at 600°C/4 Hours

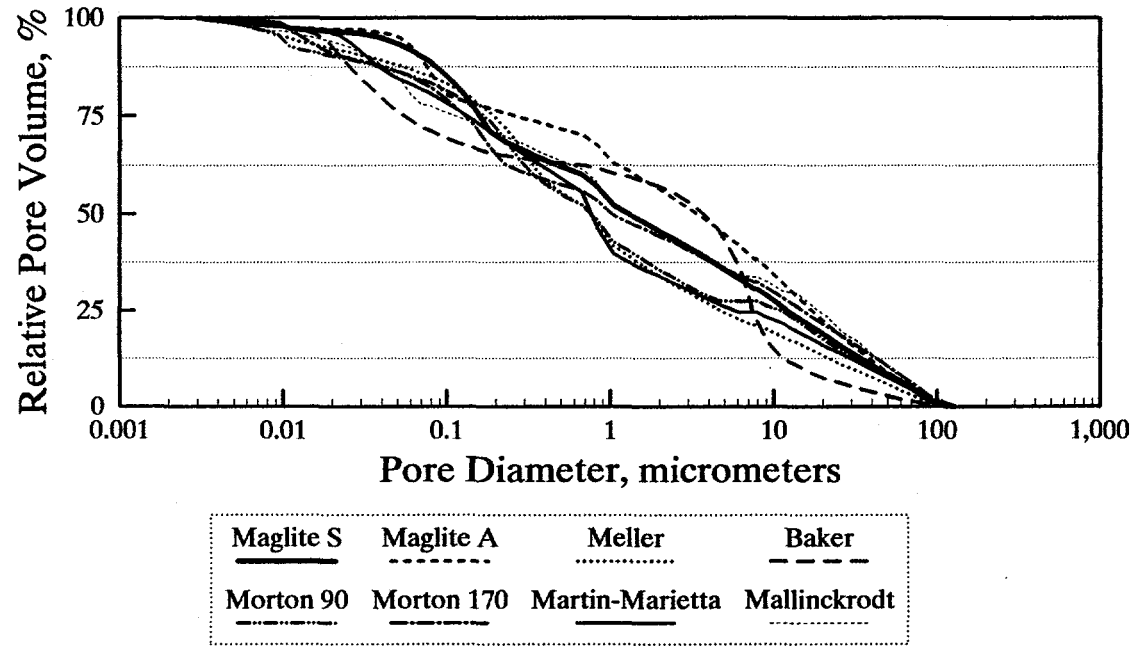

FIGURE 15. Pore-Size Distribution of MgO Powders on Relative (Normalized) Basis After Calcining at 600°C/4 Hours

TABLE 5. Median Pore Sizes of MgO Powders (Volume Basis)

MgO Source	Median Pore Size, μm
Maglite S	1.29
Morton 90	0.77
Maglite A	3.40
Baker	0.75
Morton 170	1.02
Mallinckrodt	1.35
Martin-Marietta	0.77
Meller	3.71
MAGOX 90HR	N.A.
MAGOX 98HR	N.A.

MgO had a higher deformation than the corresponding EB made with Maglite S MgO. Still, the EB with Maglite A MgO ranked third in deformation characteristics. Only 5% of the pores for the Maglite S and A MgO powders were less than 0.05 micrometers, while the corresponding value for the other MgO powders was about 10%. No other characteristics of the pore-size distribution curves appeared obvious in terms of the Maglite S MgO exhibiting deviant behavior.

MgO Calcining Temperature. All the MgO powders used in the study were calcined at 600°C for four hours to decompose carbonate and hydroxide impurities. The use of higher calcining temperatures can have an impact upon the resulting EB mixes made with the MgO, by changing the sample morphology or pore-size distribution. This effect was examined with the Maglite S MgO, by calcining the material at temperatures of 600°C to 900°C in 100°C increments.

The change in surface area with calcining temperature is shown in Figure 16. The surface area dropped dramatically due to sintering when the calcining temperature exceeded 700°C. This is readily evident in the sample morphologies shown in the SEM photomicrographs of Figures 17, 18, and 19 for temperatures of 700°C, 800°C, and 900°C, respectively. These sample morphologies can be compared in Figure 4 to that of the MgO calcined at the standard temperature of 600°C.

The onset of sintering was evident for the sample heated at 800°C (Figure 18). Substantial sintering occurred when the calcining temperature was increased to 900°C (Figure 19). As will be discussed later, this had a profound impact upon EB pellets subsequently made with these materials.

NMR Study. Several pieces of information are obtained from the spin-lattice NMR relaxation experiments: the magnitude of the equilibrium magnetization (M_0) and the average relaxation decay constant, T_1. M_0 provides a measure of the total proton density of the sample, i.e., the amount of adsorbate (*n*-heptane, in this case) that is present. These parameters provide a means of estimating the active pore area of the material.

The data from the NMR experiments are summarized in Table 6. There was no correlation to the ranking of the MgO materials in terms of their effectiveness as binders for molten salts. This technique does not appear useful for the purposes of this study.

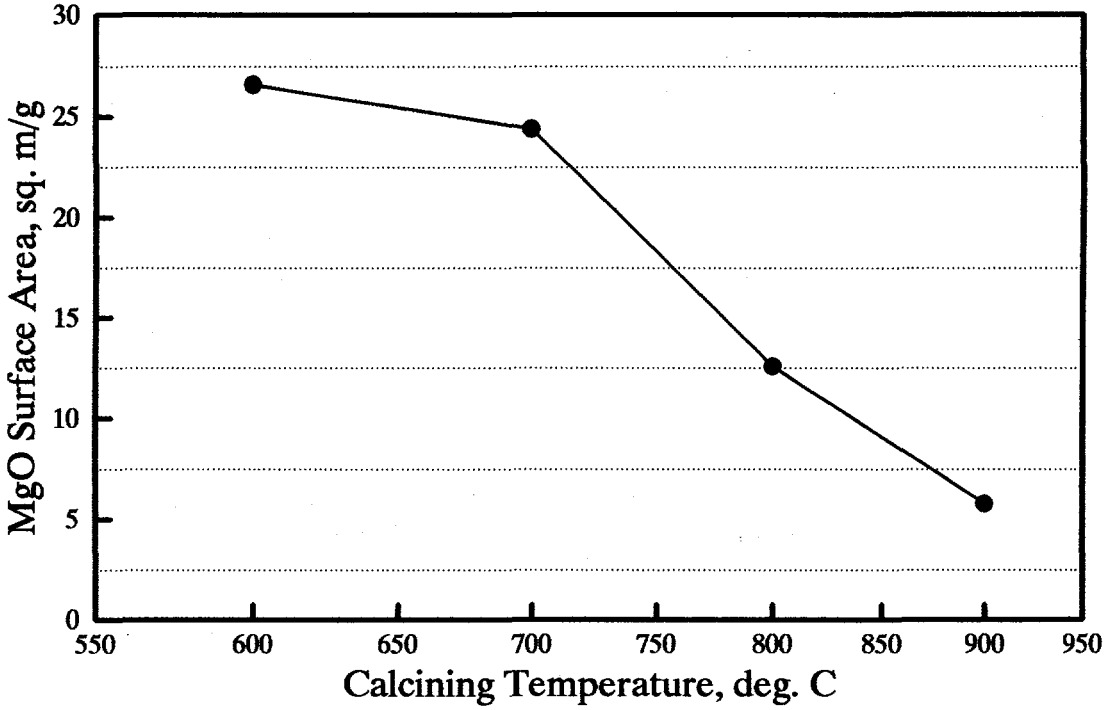

FIGURE 16. Surface Area of Maglite S MgO as a Function of Calcining Temperature

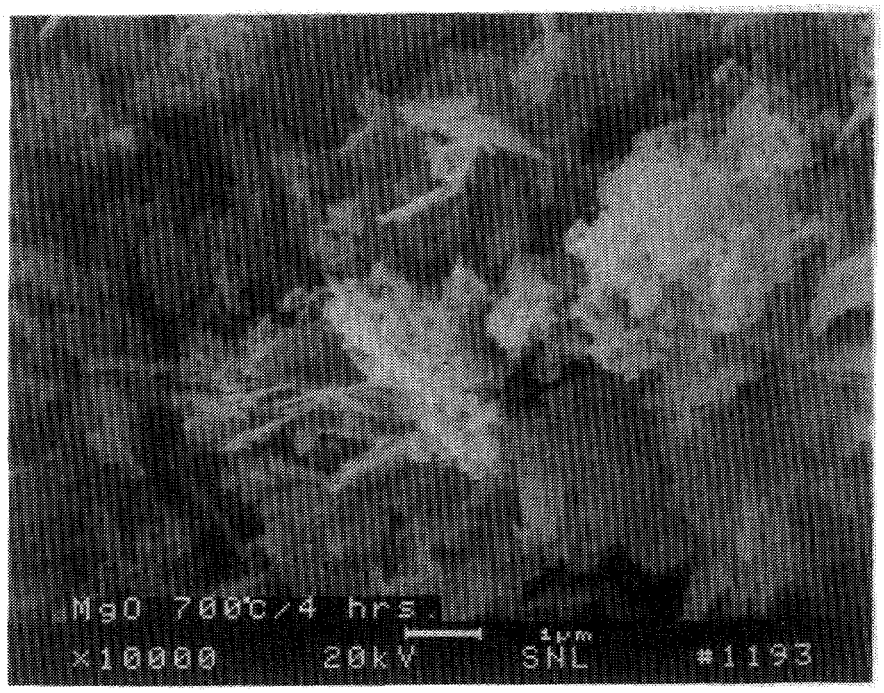

FIGURE 17. SEM Photomicrograph of Maglite S MgO Calcined at 700°C/4 Hours

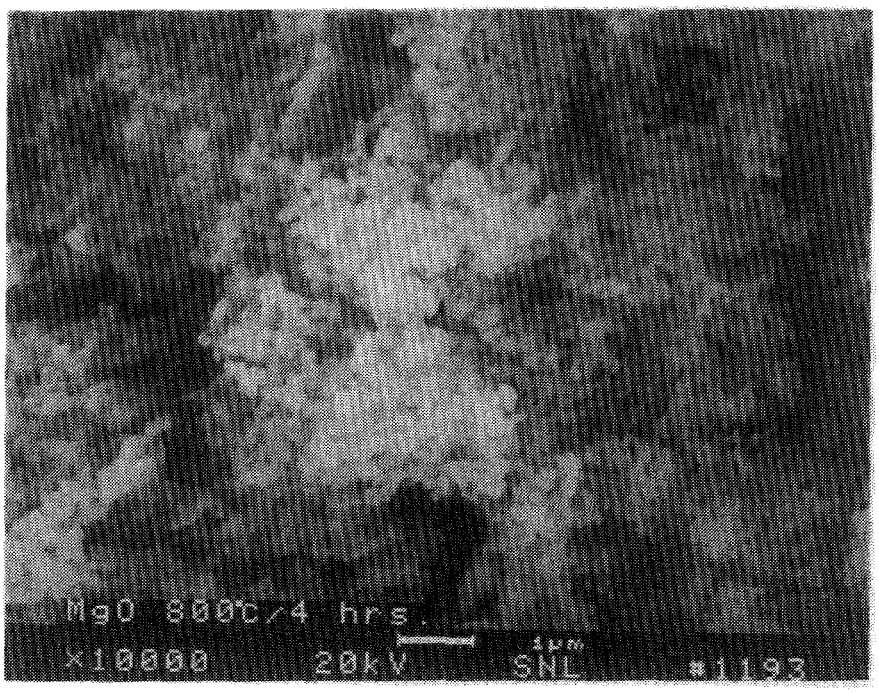

FIGURE 18. SEM Photomicrograph of Maglite S MgO Calcined at 800°C/4 Hours

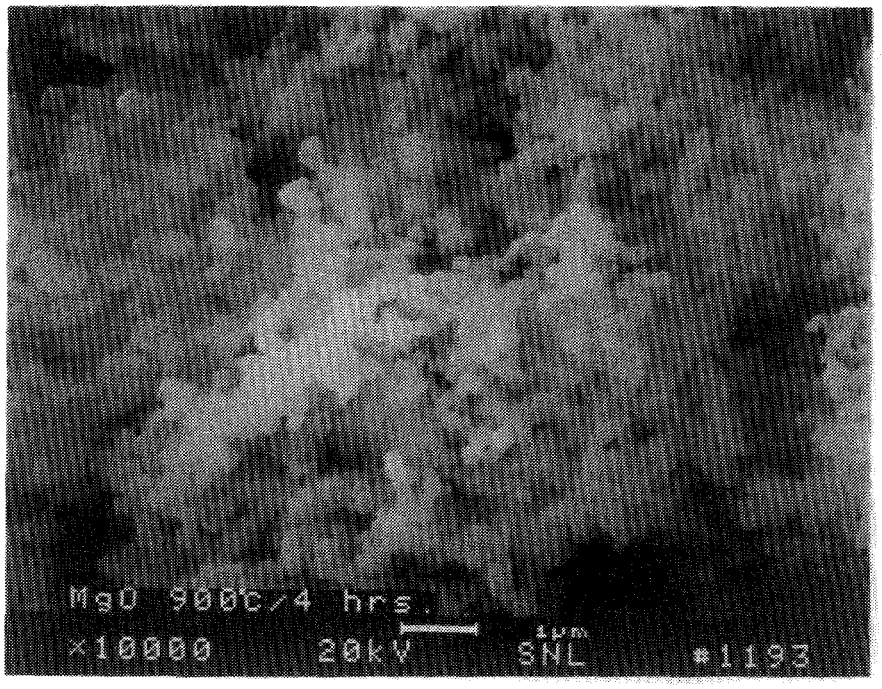

FIGURE 19. SEM Photomicrograph of Maglite S MgO Calcined at 900°C/4 Hours

TABLE 6. Summary of NMR Experiments with MgO Powders

MgO	M_0	Avg. T_1, s
Maglite S	327	0.544
Morton 90	404	1.095
Maglite A	458	1.856
Baker	317	1.399
Morton 170	434	0.108
Mallinckrodt	632	2.081
Martin-Marietta	304	0.211
Meller	1078	1.833

TABLE 7. Surface Area of EB Mixes Made with 35% MgO and Fused at 400°C/16 Hours

MgO Source	EB Surface Area, m^2/g
Maglite S	1.12
Morton 90	0.89
Maglite A	0.34
Baker	0.26
Morton 170	0.71
Mallinckrodt	0.82
Martin-Marietta	0.81
Meller	0.42

Characterization of EB Powders

Surface Area. The surface areas of the EB mixes made with the various MgO powders are listed in Table 7, in decreasing ranking of their effectiveness as a binder for molten salt. There was no correlation of the deformation ranking with the EB surface area. While the Maglite S EB had the highest surface area, the deformation of three EBs with similar surface areas (*viz.*, the ones with Norton 90, Mallinckrodt, and Martin-Marietta MgOs) varied widely in their deformation properties.

Angle of Repose. The angle of repose of the EB mixes made with the various MgO powders is listed in Table 8; the MgO powders are ranked in decreasing order of effectiveness as a binder for molten salt. The angles of repose for the various EBs showed no correlation to the deformation properties. For example, the angle of repose for the EB with the highest deformation–that made with Meller MgO–was similar to those of the EBs that exhibited much more moderate deformation (*e.g.*, that made with Baker MgO).

TABLE 8. Angle of Repose of EB Mixes Made with 35% MgO and Fused at 400°C/16 Hours

MgO Source	Angle of Repose, degrees
Maglite S	62.3 ± 1.8
Morton 90	63.9 ± 1.8
Maglite A	49.8 ± 2.5
Baker	46.2 ± 1.5
Morton 170	61.9 ± 2.8
Mallinckrodt	62.7 ± 1.8
Martin-Marietta	58.7 ± 0.82
Meller	46.0 ± 0.42

While not useful for predicting the deformation characteristics of a powder, the angle of repose is a good metric for the *flow properties* of a powder. A high angle of repose indicates poor flow properties. The EB made with Maglite S MgO had the

highest angle of repose of all the EBs measured and, consequently, the poorest flow properties. A lower angle of repose means that the powder will fill the die cavity much more readily during pressing of pellets. This greatly facilitates the pelletizing operation and reduces the tendency for density gradients throughout the separator pellet.

Melting/Freezing Points. The onset of melting and freezing of the various EB mixes was measured by DSC to try to correlate these data with the tendency for deformation. The thermal data are summarized in Table 9, with the EBs ranked in decreasing effectiveness of the respective MgO powder to immobilize the molten electrolyte. (For comparison, data are also included for pure LiCl-KCl eutectic.)

Materials with a higher level of impurities that might be soluble in molten LiCl-KCl eutectic would be expected to show an increased depression of the melting point. The onset of freezing, however, can be lower than the onset of melting due to supercooling of the melt. This is evident for even the pure LiCl-KCl eutectic.

Examination of the data shows that there is no consistent trend with the observed melting points and the effectiveness of the MgO to immobilize the molten salt. There was also no direct correlation with the level of impurities in the MgO (see Table A-1 and A-2 in Appendix A). Not all the impurities would be expected to dissolve in the molten LiCl-KCl eutectic and thus cause a depression of the melting point.

NMR Study. The data from the limited NMR experiments with EB powders are summarized in Table 10. There was no correlation of the characterization parameters for sorption (M_0 and T_1) to the ranking of the EB powders in terms of the effectiveness of the corresponding MgO as a binder for molten salts. The EB with Maglite S MgO, for example, has a value of M_0 identical to that for one the EB with Meller MgO–similar values of M_0 for MgOs at opposite ends of the spectrum for immobilization efficiency. Similar results were obtained with the pure MgO powders (Table 6), reinforcing the premise that this technique does not apear useful for the purposes of MgO characterization.

Particle-Size Distribution. The relative particle-size distributions of the EB mixes made with the various MgO powders are summarized in Figure 20. Except for the EBs based on Maglite S and Morton 90, the particle-size distributions tended to cluster around a median particle size of 20-25 micrometers. The EB with Maglite S MgO

TABLE 9. Onset of Melting/Freezing of EB Mixes Made with 35% MgO and Fused at 400°C/16 Hours

MgO Source	Onset of Melting, °C	Onset of Freezing, °C
Maglite S	346.5	344.5
Morton 90	348.0	344.0
Maglite A	348.0	344.0
Baker	349.5	346.5
Morton 170	348.2	343.2
Mallinckrodt	350.5	345.0
Martin-Marietta	350.0	345.3
Meller	348.5	345.0
LiCl-KCl eut.	352.2	347.0

TABLE 10. Summary of NMR Experiments with EB Powders

MgO	M_0	Avg. T_1, s
Maglite S	481	1.474
Morton 90	535	1.467
Maglite A	689	1.526
Baker	642	0.732
Morton 170	682	1.451
Mallinckrodt	358	0.954
Martin-Marietta	608	1.097
Meller	481	1.923

had the smallest median particle size of ~8.5 micrometers, while the EB with Morton 90 MgO had a median particle size of ~15 micrometers. There does not appear to be a correlation of the particle-size distributions of the EBs made with the various MgO powders with the ranking of the EBs based on deformation properties.

Pore-Size Distribution. The relative pore-size distributions of the EB mixes made with the various MgO powders are summarized in Figure 21 on a volume basis and in Figure 22 on a relative (normalized) basis. The striking feature of the EB made with Maglite S is that it had a much smaller median pore-size compared to the other EBs–only 0.4 micrometer vs. greater than 1 micrometer, respectively.

The second smallest median pore size was for the EB made with Morton 90; this EB

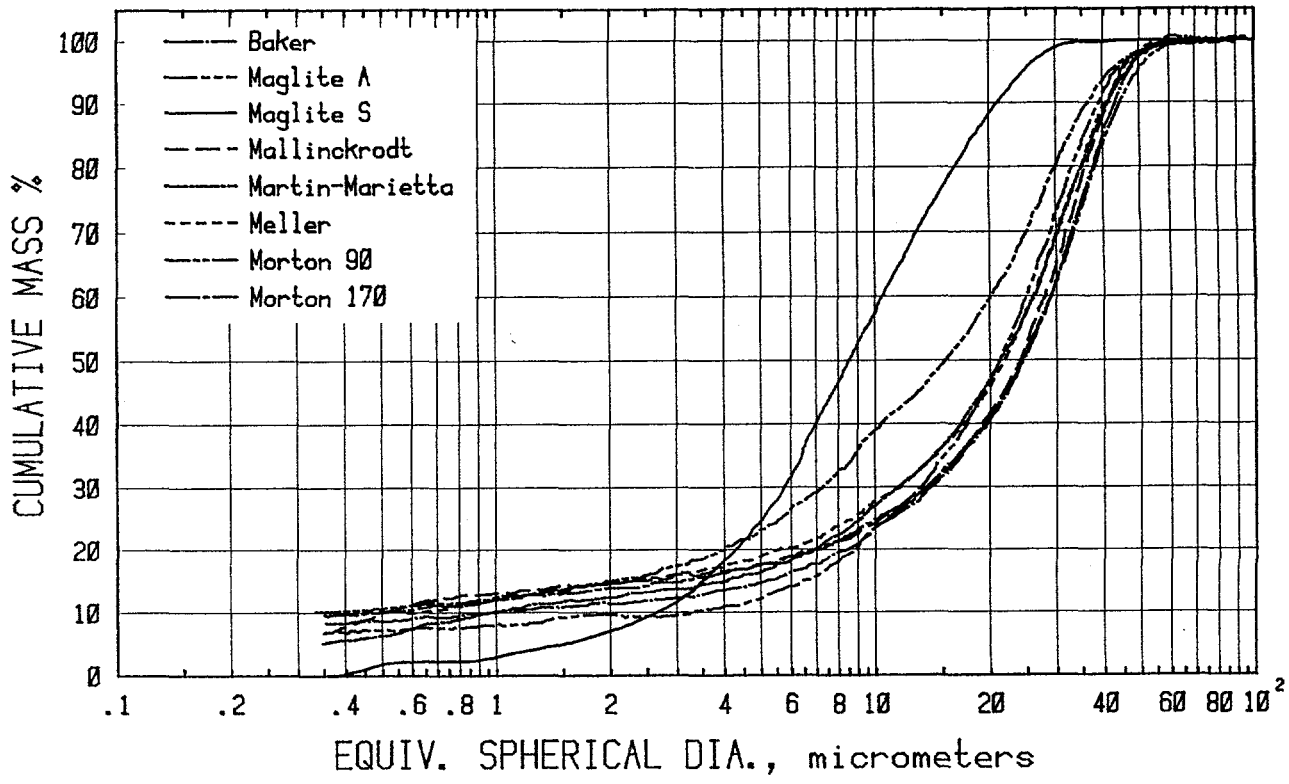

FIGURE 20. Particle-Size Distribution of EB Powders Made with Various MgOs

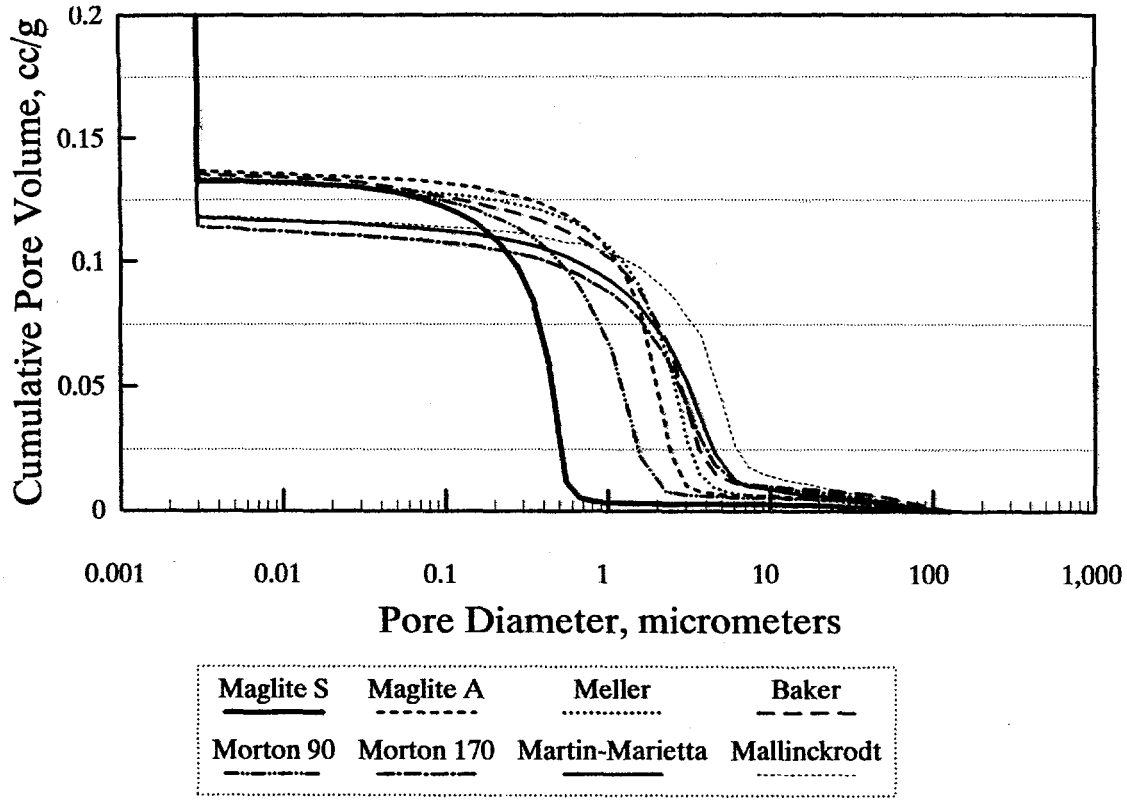

FIGURE 21. Pore-Size Distribution of EB Powders on Volume Basis

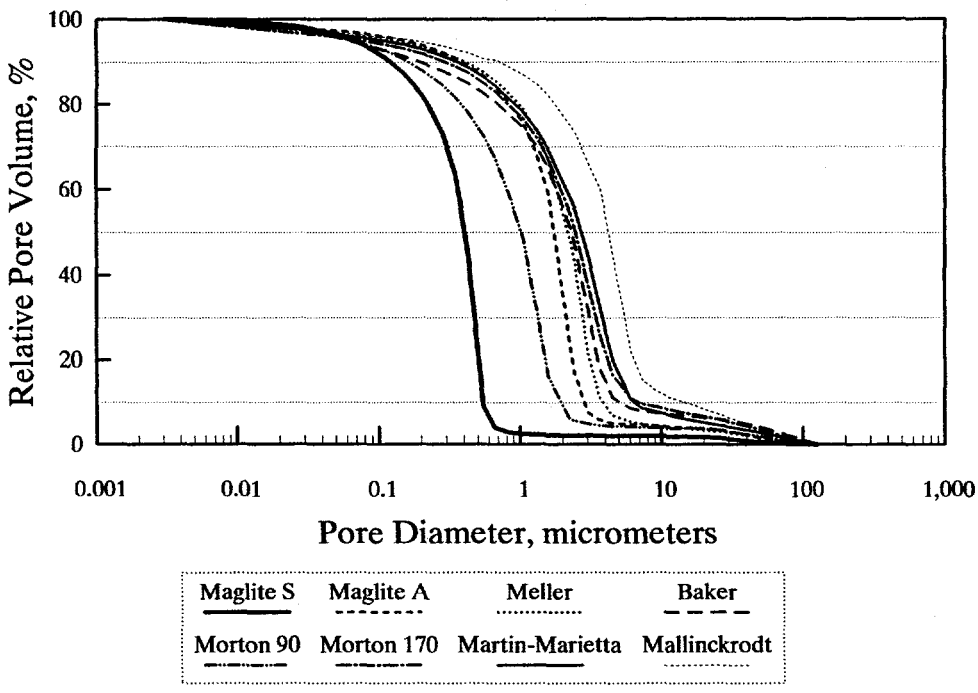

FIGURE 22. Pore-Size Distribution of EB Powders on Relative (Normalized) Basis

also was ranked as second best in its deformation properties. The third smallest median pore size was for the EB made with Maglite A, which was correspondingly ranked as the third best in its deformation characteristics. At least for the top three materials, the pore-size distribution of the EB mixes correlates with their deformation. However, this still doesn't correlate to a specific intrinsic property of the MgO powders themselves as to **why** this behavior is observed. This may be related to the amount of pores under 0.5 micrometers (Figure 15).

EB Fusion Temperature. As was mentioned earlier, the temperature can significantly have an impact on the wetting process during EB fusion. The effect of EB fusion temperature was examined briefly to gather information concerning this important step in EB processing. The data are summarized in Figure 23 for EBs prepared with 35% Maglite S MgO.

The EB surface area increased substantially (doubled) when the fusion temperature was reduced to 375°C, which is only 23°C above the melting point. This indicates that there was reduced access to the some of the pores of the MgO at the lower temperature; i.e.,the wetting was reduced. (This affected the deformation of the pellet, as will be discussed later.) There was little change, however, when the temperature was increased to 425°C. This suggests that further access to the pores of the MgO was not enhanced at the higher temperature.

MgO Calcining Temperature. The surface areas of EB mixes made with Maglite S MgO calcined at temperatures above 600°C were measured, for possible correlation to the resulting deformation properties of these materials. The EB surface-area data are summarized in Figure 24 as a function of the calcining temperature of the MgO. The surface area reached a maximum near 700°C and then dropped off rapidly at higher temperatures. This trend is somewhat different from that shown by the surface area of the MgO as a function of calcining temperature (Figure 16), where no maximum was observed.

Characterization of EB Pellets

Deformation. The deformation characteristics of the various EB mixes were listed previously in Table 3 for an MgO content of 35%. These data were for pellets pressed to ~75% of theoretical density (TD) (25% porosity), a temperature of 530°C, and an applied pressure of 99 kPa (14.3 psig). The density of the pellets and applied pressure have been shown to have a significant impact upon the deformation.[3]

The effect of ***binder content*** upon the deformation is shown in Figure 25. The deformation dramatically increased when the MgO content was reduced below 35%.

The effect of EB ***fusion temperature*** upon pellet deformation is shown in Figure 26 for the EB with 35% Maglite S MgO. The deformation dropped considerably when the fusion temperature was decreased by 25°C from the nominal 400°C. The deformation increased only slightly when the fusion temperature was increased to 425°C. The lower fusion temperature is only 23°C above the melting point of the electrolyte. In contrast, the higher fusion is 73°C above the melting point of the LiCl-KCl eutectic. Changes in the wetting properties of the molten electrolyte at the fusion temperature of 375°C and 425°C are probably responsible

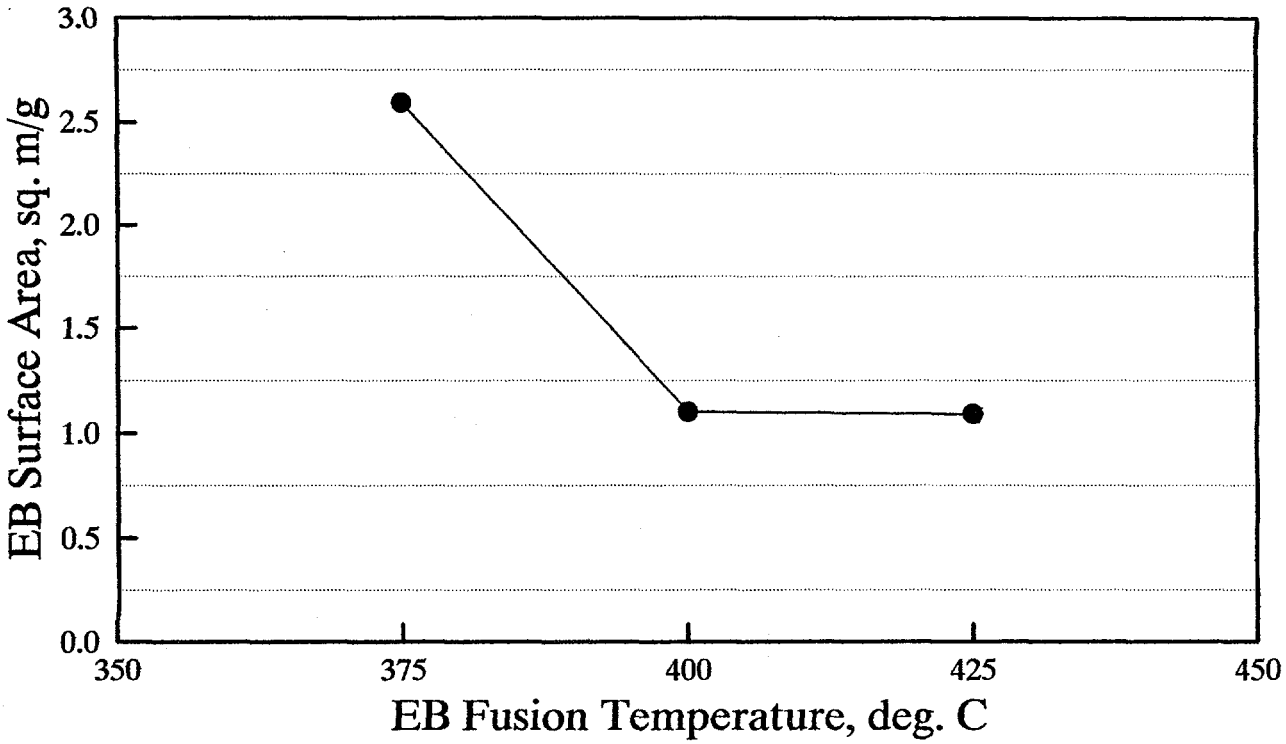

FIGURE 23. Surface Area of EB Mixes as a Function of EB Fusion Temperature

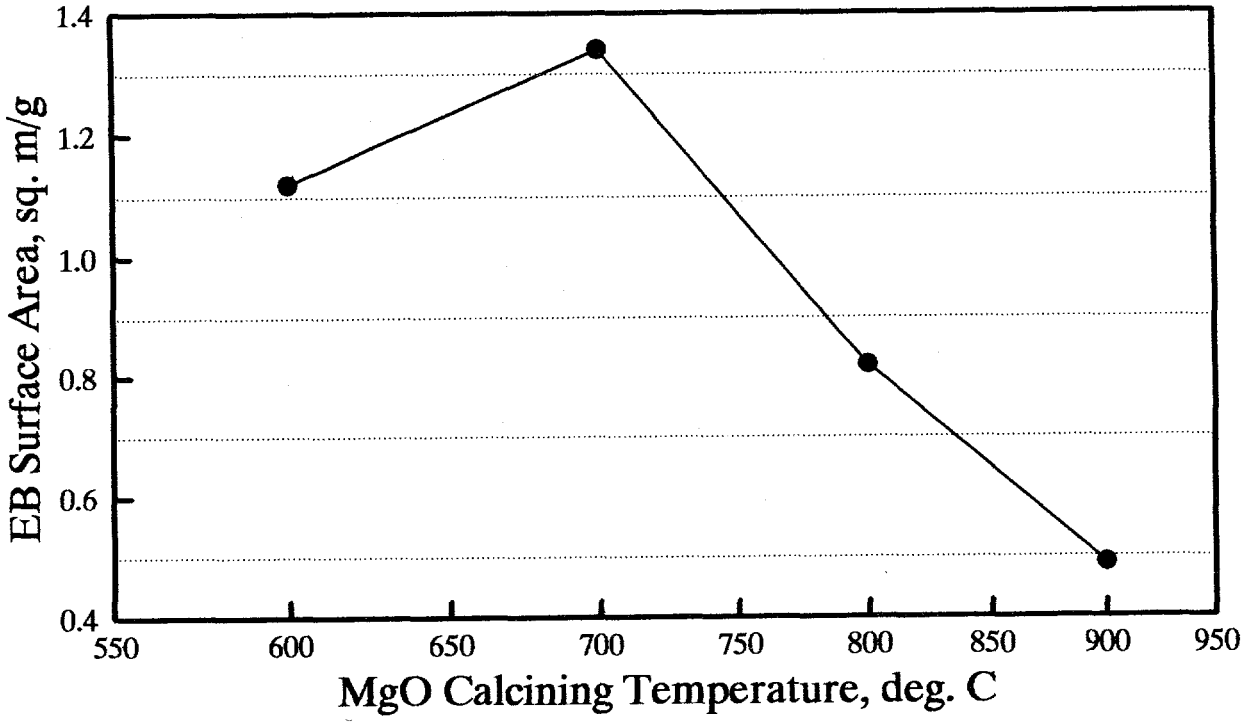

FIGURE 24. Surface Area of EB Mixes as a Function of MgO Calcining Temperature

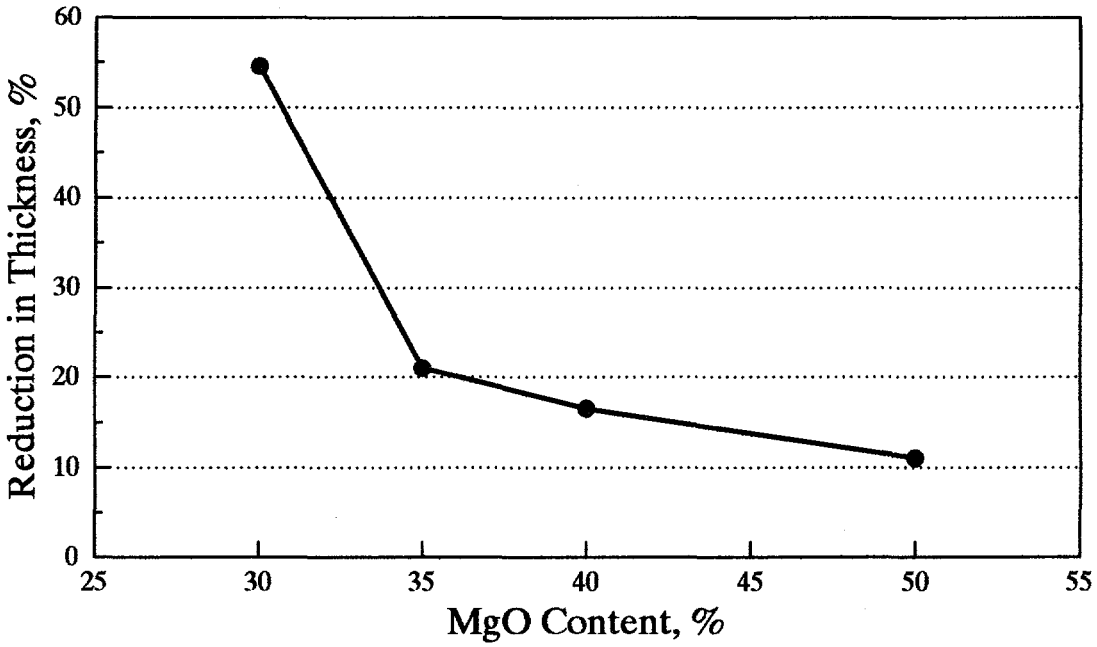

FIGURE 25. Deformation as a Function of MgO Content for EB Pellets Made with Maglite S MgO and LiCl-KCl Eutectic

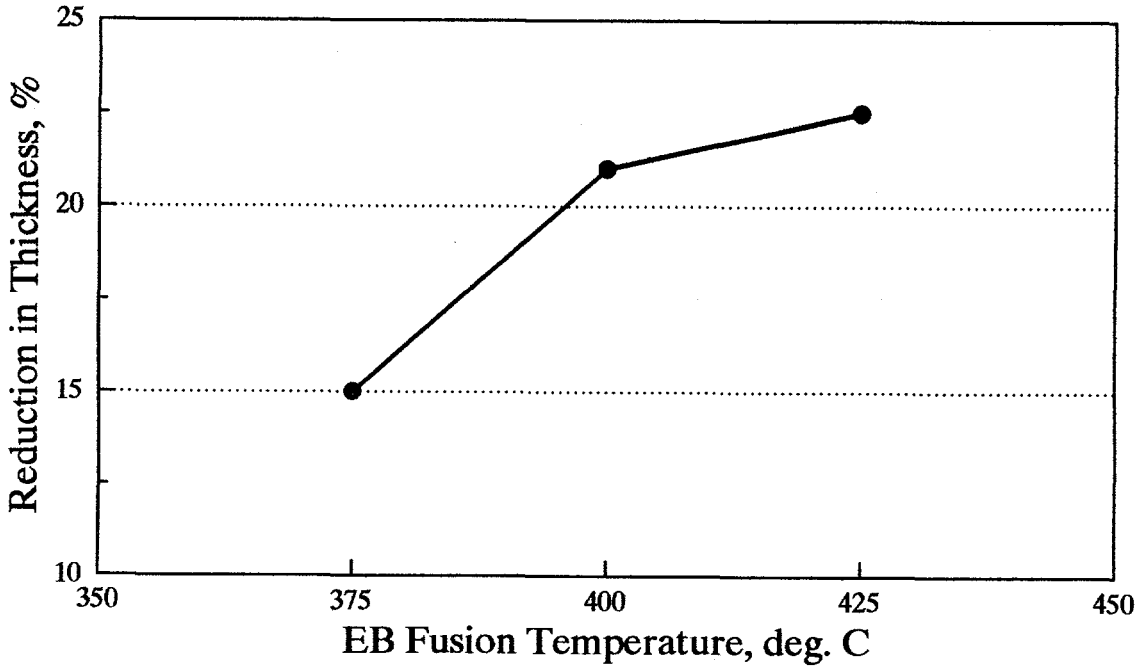

FIGURE 26. Deformation as a Function of EB Fusion Temperature for EB Pellets Made with 35% Maglite S MgO and LiCl-KCl Eutectic

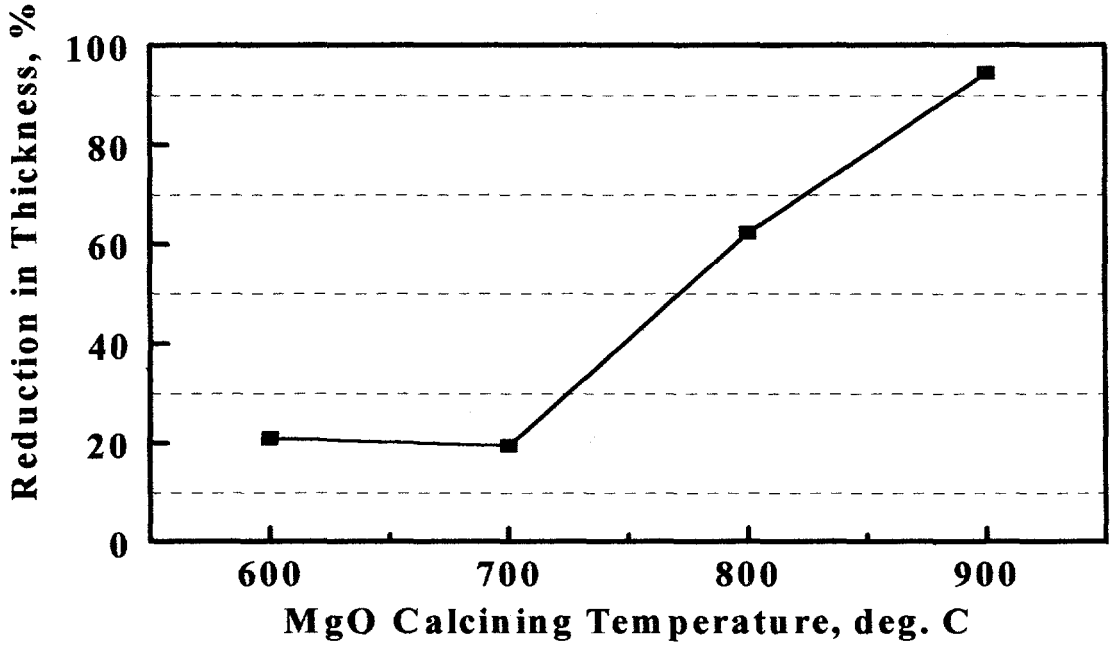

FIGURE 27. Deformation as a Function of MgO Calcining Temperature for EB Pellets Made with 35% Maglite S MgO and LiCl-KCl Eutectic

for the observed differences in the EB deformation.

If one examines the BET ***surface areas*** over this temperature range used for EB fusion (Figure 23), one observes an inverse relationship with the deformation behavior (Figure 26). As the EB-fusion temperature increases, the surface area decreases but the deformation increases.

The effect of MgO ***calcining temperature*** upon the EB deformation is shown in Figure 27 for EBs made with 35% Maglite S and fused at 400°C for 16 hours in the dry room. There was a rapid increase in deformation when the calcining temperature exceeded 700°C. Both the surface area of the MgO and that of the corresponding EB show an inverse relationship with the MgO calcining temperature (Figures 16 and 24, respectively).

As previously mentioned, the ***density*** of the EB pellets affects its deformation behavior. If the density is too low, the pellet tends to show a large reduction in thickness upon melting due to the collapse of the large amount of void space. On the other hand, excessively high densities results in too little void space to retain the electrolyte once it becomes molten, resulting in a large reduction in thickness accompanied by a concomitant flow of material in the radial direction. Figure 28 shows the dependency over a moderate range of densities for the deformation of EB pellets made with 35% Maglite S MgO and LiCl-KCl eutectic. Above ~75% TD, the deformation dramatically increases.

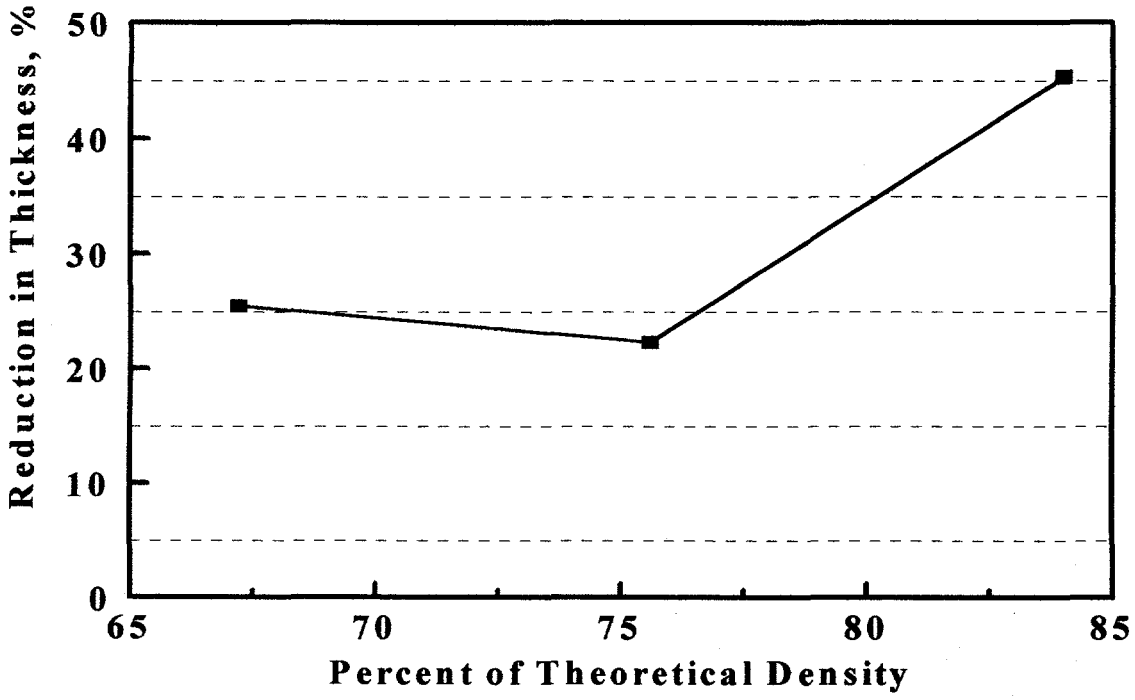

FIGURE 28. Deformation as a Function of Percent of Theoretical Density for EB Pellets Made with Maglite S MgO and LiCl-KCl Eutectic

TABLE 11. Electrolyte Leakage of EB Pellets Made with 35% MgO and LiCl-KCl Eutectic*

MgO Source	Electrolyte Leakage, mg/cm^2
Maglite S	6.48 ± 0.10
Morton 90	9.78 ± 0.12
Maglite A	12.0 ± 1.15
Baker	14.3 ± 1.30
Morton 170	14.7 ± 0.62
Mallinckrodt	22.3 ± 1.05
Martin-Marietta	20.2 ± 0.69
Meller	25.1 ± 0.20

* Samples heated in dry-room furnace at 400°C for 0.5 h in bed of alumina.

Electrolyte Leakage. The electrolyte leakage of the EB pellets made with the various MgO powders is summarized in Table 11, with the MgOs ranked in decreasing order of effectiveness in immobilization of molten electrolyte. The top four EBs with the lowest deformation were also the top four ones with the lowest electrolyte leakage. However, the relative order was not related directly to the deformation ranking. Maglite S was again the best, exhibiting the lowest leakage and deformation. Except for the EB made with Morton 170 MgO, the EBs with deformation more than 58% were grouped together, showing similar leakages.

The effect of Maglite S ***MgO content*** upon the electrolyte leakage of EB pellets is

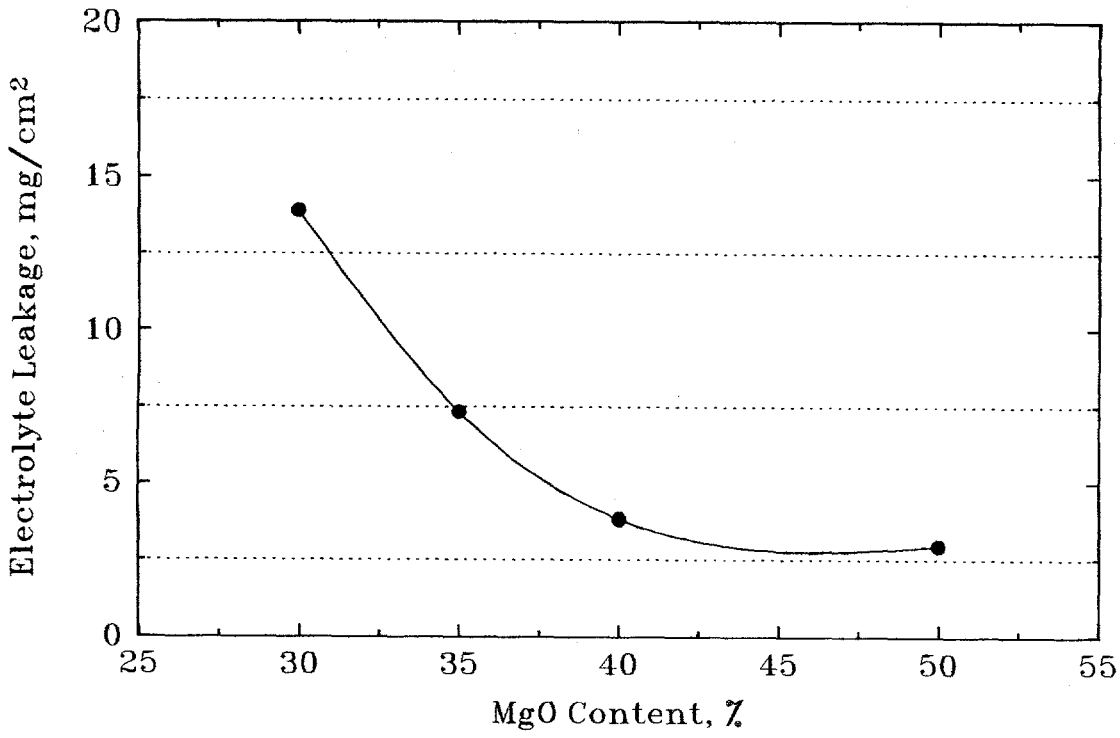

FIGURE 29. Electrolyte Leakage as a Function of MgO Content for EB Pellets Made with Maglite S MgO and LiCl-KCl Eutectic

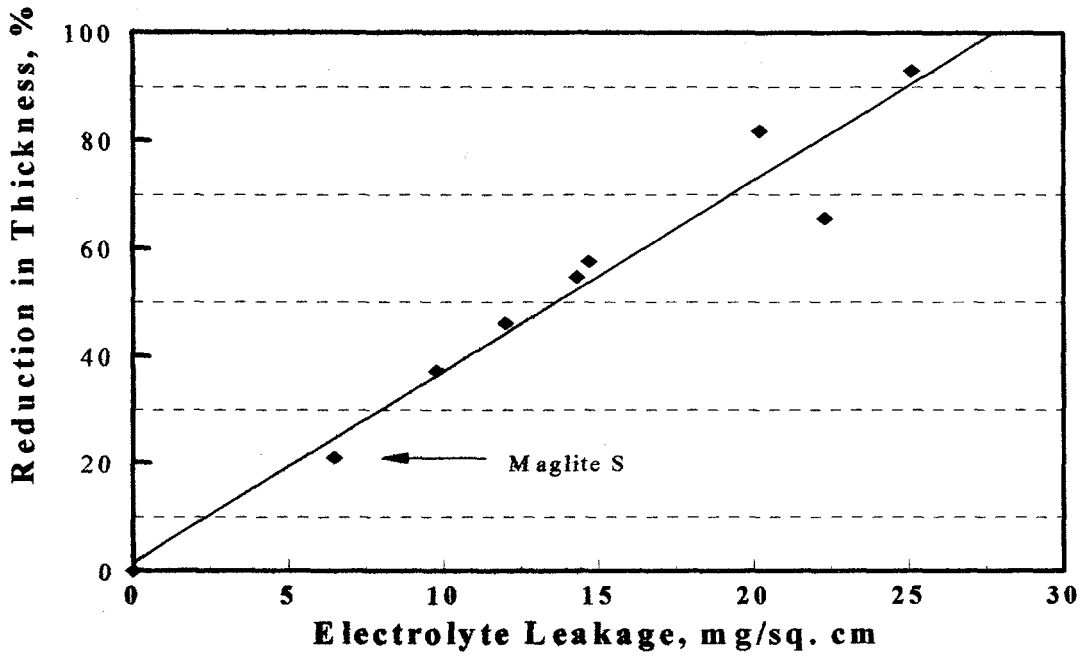

FIGURE 30. Deformation as a Function of Electrolyte Leakage for Various EB Pellets Made with 35% MgO and LiCl-KCl Eutectic

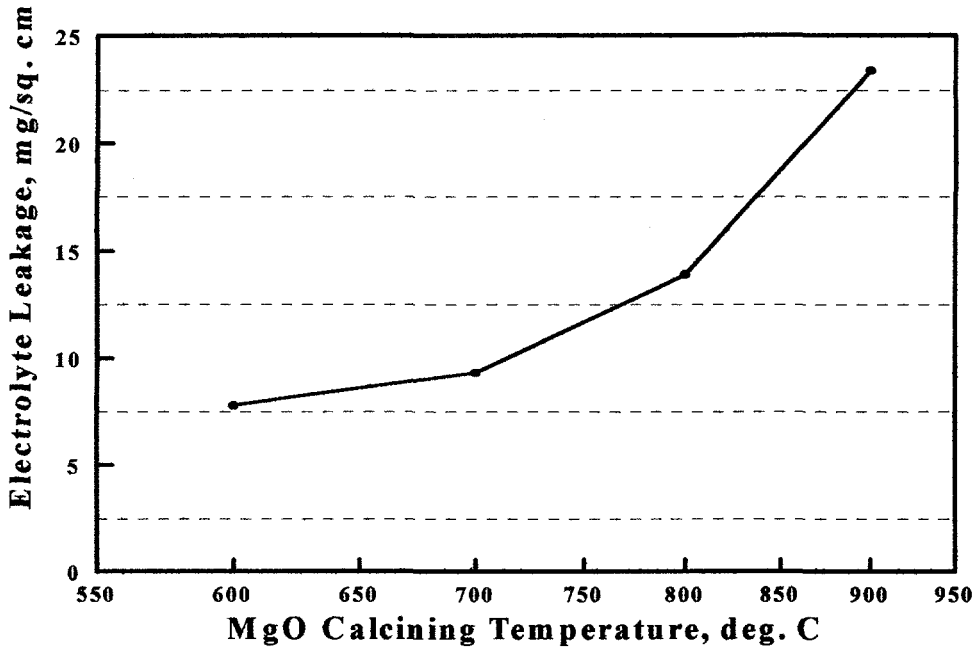

FIGURE 31. Electrolyte Leakage as a Function of MgO Calcining Temperature for EB Pellets Made with 35% Maglite S MgO and LiCl-KCl Eutectic

shown in Figure 29. The electrolyte leakage dropped to a plateau near 40% MgO. This is comparable to the trend observed for the deformation behavior of these pellets above 35% (Figure 25). This close linkage in behavior of these two parameters is evident in Figure 30, which plots the deformation behavior of the various EB pellets (with 35% MgO) against the observed electrolyte leakage at 400°C. The correlation of these two parameters is fairly good ($r^2 = 0.94805$).

The electrolyte leakage of EBs made with 35% Maglite S is shown in Figure 31 as a function of MgO ***calcining temperature***. The rapid increase in electrolyte leakage at calcining temperatures above 700°C correlates well with the similar effect observed in the deformation behavior of these pellets (Figure 27).

The effect of pellet ***density*** upon the leakage of EB pellets made with 35% Maglite S MgO is shown in Figure 32. The leakage exhibited a minimum near 67% TD. The corresponding deformation behavior was quite similar, in that there was a rapid rise in deformation above ~75% TD (Figure 28).

Discussion

Processing implications

The deformation with fusion temperature of the EB containing 35% Maglite S MgO (Figure 26) suggests that control of this parameter is important from a production standpoint. A negative deviation of 25°C below the 400°C specification temperature can lead to a slight increase in the surface area of the EB powder and a reduction in pellet deformation from ~21% to 15%. A positive of 25°C above the 400°C

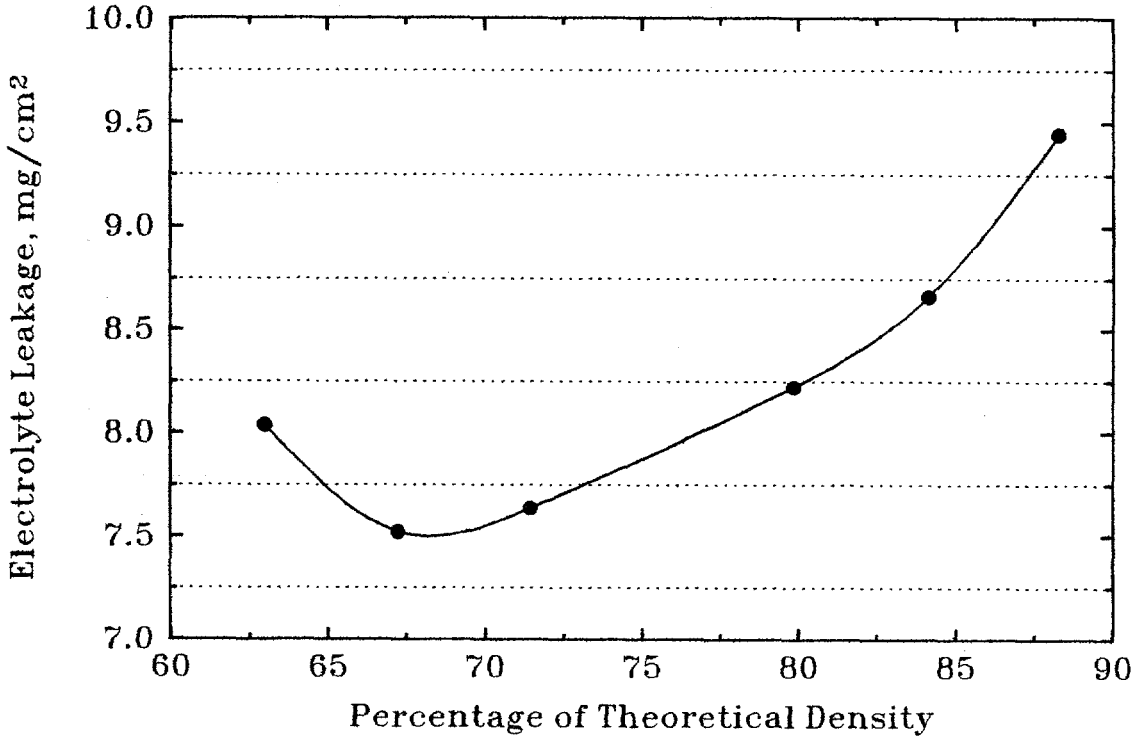

FIGURE 32. Electrolyte Leakage as a Function of Percent of Theoretical Density for EB Pellets Made with 35% Maglite S MgO and LiCl-KCl Eutectic

temperature will lead to a slight reduction in the EB surface area and a slight increase in the pellet deformation to ~22.5%. Maintaining the EB fusion temperature within the 375°-425°C window is not likely to cause any problems for this material, since these observed deformation values lie well within the acceptable region. Overshooting of the fusion temperature is not as likely to have negative ramifications as undershooting for this EB composition.

Too low of a deformation value can cause different kinds of problems in performance compared to excessive deformation. In the latter case, failure can occur through excessive electrolyte leakage and the formation of parasitic currents between adjacent cells. In the former case, reduced wetting at the separator-anode and separator-cathode interface can lead to increased interfacial resistance which will give rise to a higher battery impedance.

At this time, the two most powerful tools for characterization of MgO powders for use in thermal-battery separators are the deformation and electrolyte leakage of EB pellets. These parameters track each other quite well, as can be seen in Figure 30. Neither requires sophisticated electronics nor hardware to implement. The electrolyte-leakage test is by far the simpler. These techniques are also useful for quality-control purposes and for troubleshooting problems related to the separator mixes.

Pore-Size Effects

The various properties of the MgO powders

that we evaluated were not readily correlated to the behavior of these materials when formulated into EB mixes for use in thermal batteries. The only MgO characterization parameter that had any kind of general correlation to this parameter was the pore-size distribution. The reduced amount of pores under 0.5 micrometers appeared to be distinct for the Maglite S and Maglite A MgO powders.

The viscosity and surface tension of the molten salt will determine how much of the available porosity of the MgO powder will be accessible to it during the EB fusion step. These, in turn, are affected by temperature and electrolyte purity. A MgO powder with a high number of large pores (*e.g.*, Meller MgO) will have most of these flooded by the molten salt during the initial EB fusion. Consequently, when EB pellets made from this material are melted under an applied pressure (*e.g.*, as a separator in a thermal battery upon activation), they will exhibit excessive deformation. In addition, there will be a tendency for the electrolyte to leak from the EB, as there will be little residual capacity to absorb the liquid-salt phase.

Conversely, a MgO powder with a fair number of smaller pores (*e.g.*, Maglite S MgO) will have a greater residual porosity available after the EB fusion step, since all of the major pores will not be flooded; *i.e.*, the depth of pore penetration will be less with smaller pores. As a result, it will have a built-in capacity to absorb electrolyte when EB pellets made from it are subjected to the same dynamic environment. The distribution of the pore sizes ultimately will determine how the MgO powder will behave when used as a binder for molten salts in a thermal-battery environment.

Replacement for Maglite S MgO

Since the molten electrolyte is held in place in the MgO powder by capillary action, it makes sense that the pore-size distribution plays a critical role in this process. The other parameters that influence the wetting process (*e.g.*, impurities in the MgO) do not appear to be a deciding factor, based on the data generated in this study. Thus, a direct MgO replacement of the Maglite S should have a pore-size distribution that is as similar as possible to that of the Maglite S MgO.

During this characterization study, the manufacturer of Maglite S MgO announced that it would no longer be available commercially. This gave us a strong incentive to immediately find a suitable replacement. An alternate source that the manufacturer recommended was Marinco 'OL' MgO from Marine Products Co. (Coraopolis, PA). This material is currently under evaluation.

Preliminary data from mercury-porosimetry measurements show the pore-size distribution for Marinco OL MgO to be quite similar to that for Maglite S MgO. The sample morphology appears comparable, as well, as seen in Figure 33 which is an SEM photomicrograph of this material after calcining at 600°C for fours hours. (Compare this to Figure 4 which is the corresponding SEM photomicrograph of Maglite S MgO.)

These data suggest that Marinco OL MgO will very likely be a suitable replacement for Maglite S MgO for use as a binder for molten electrolytes in the separators of thermal batteries. This is corroborated by preliminary electrolyte-leakage and pellet-deformation tests with an EB mix made with 35% Marinco OL MgO and LiCl-KCl eutectic electrolyte. Some adjustment in

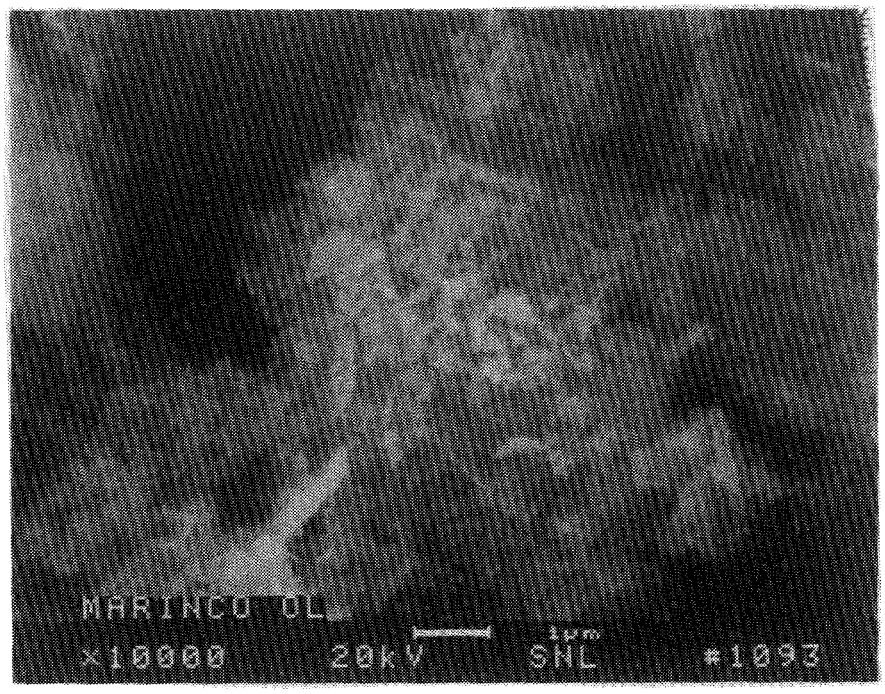

FIGURE 33. SEM Photomicrograph of Marinco OL MgO After Calcining at 600°C/4 Hours

formulation may be necessary, however, for different electrolyte composition.

Most of the other MgO powders examined would not be suitable at level of 35% as was Maglite S. Some of these materials could still be used, however, if the binder level in the EB were increased to effect better immobilization. The exact level necessary can readily be determined by preparation of EBs with increasing MgO levels and measuring the deformation or electrolyte leakage of pellets made from these mixes. The appropriate MgO level is defined by the minimum amount necessary for EB deformation or electrolyte leakage that is comparable to those exhibited by the standard EB mix. (In this case, 35% Maglite S MgO and LiCl-KCl eutectic electrolyte.) Too high a binder content, however, can adversely impact the ionic conductivity of the separator pellet.

Mixes that use other electrolytes, such as the all-Li LiCl-LiBr-LiF minimum-melting electrolyte or the low-melting LiBr-KBr-LiF eutectic will also have to be re-evaluated if Maglite S MgO is replaced with Marinco OL MgO.

Conclusions

Ten commercial MgO powders were evaluated for use as a binder for LiCl-KCl eutectic electrolyte in the separator of thermal batteries. Out of 10 materials evaluated, Maglite S was superior by far. EBs made with Maglite S MgO showed the least deformation and electrolyte leakage and had the largest surface areas and smallest median pore size (volume basis).

Select physical and chemical properties of the MgO materials were evaluated for possible correlation to the deformation

properties of EB pellets made with them. (The deformation behavior is the primary characterization criterion for MgO qualification.) These included purity, surface area, particle-size distribution, morphology, and pore-size distribution. Except for the latter two (which are interrelated), none could be correlated to the deformation data. The Maglite S MgO was the only one with a bimodal particle-size distribution. The unique pore-size distribution of the Maglite S MgO is responsible for its excellent binding properties for immobilization of molten electrolyte by capillary action. Consequently, this makes it ideally suited for use in the separator of thermal batteries.

Characterization of EB powders for surface area, flow properties, melting/freezing points, particle-size distribution, and pore-size distribution showed no obvious relationship to the deformation properties of EB pellets. Attempts to follow *n*-heptane sorption by NMR relaxation techniques were not fruitful for either the EB or MgO powders in obtaining pore-characterization data.

The electrolyte leakage of EB pellets in a bed of GC-grade alumina at 400°C after 30 min was found to be another good metric for measurement of MgO binding action (electrolyte immobilization); reasonably good correlation to the deformation data was obtained. This technique is easy to carry out and does not require sophisticated equipment or skilled personnel.

The MgO content, the MgO-calcining temperature, and the EB-fusion temperature impact the deformation and electrolyte leakage of EB pellets–especially the former two. Increased deformation occurs at lower levels of MgO, higher MgO-calcining temperatures, and higher EB-fusion temperatures.

Marinco OL MgO is currently being qualified as a replacement for Maglite S MgO which is no longer being commercially produced. Preliminary pore-size data and EB-characterization data indicate that this material will likely be a suitable replacement for Maglite S MgO.

References

1. J. Q. Searcy, P. A. Neiswander, J. R. Armijo, and R. W. Bild, "Lithium Oxide in Li(Si)/FeS_2 Thermal Battery Systems," *SAND81-1705* (November 1982).
2. R. A. Guidotti and F. W. Reinhardt, "Evaluation of Alternate Electrolytes for Use in Li(Si)/FeS_2 Thermal Batteries," *Proc. 33rd Power Sources Symp.*, pp. 369-376 (1988).
3. R. A. Guidotti, F. W. Reinhardt, and E. V. Thomas, "Deformation Study of Separator Pellets for Thermal Batteries," *SAND90-2318* (May, 1995).
4. R. A. Guidotti and F. W. Reinhardt, "Characterization of Electrolyte-Binder Mixes for Use in Thermal Batteries," *SAND90-2103* (March 1991).
5. D. A. Nissen, "Processing Effects on Powders for Thermal Batteries," *SAND80-8024* (May 1980).
6. R. A. Guidotti and F. W. Reinhardt, "Characterization of DEB Powders and Pellets for Ca/$CaCrO_4$ Thermal Batteries," *SAND83-2270* (July 1985).
7. D. M. Smith, T. E. Holt, D. P. Gallegos, and D. L. Stermer, Ceramic Powder Science and Technology. Critical Aspects of Powder Characterization, *Advances in Ceramics* (1986).
8. K. Munn and D. M. Smith, *J. Colloid Interfacial Sci.*, **119(1)**, 117 (1987).

9. D. P. Gallegos, K. Munn, D. M. Smith, and D. L. Stermer, *J. Colloid Interfacial Sci.*, **119(1)**, 127 (1987).
10. F. W. Sears and M. W. Zemansky, University Physics, Part 1, 2nd ed., p. 233 Addison-Wesley, Reading, MA (1957).
11. A. W. Adamson, Physical Chemistry of Surfaces, 3rd ed., pp. 333-371, J. Wiley and Sons, New York (1976).
12. W. D. Kingery, H. K. Bowen, and D. R. Uhlmann, Introduction to Ceramics, 2nd ed., pp. 177-216 , J. Wiley and Sons, New York (1976).
13. H. M. Rootare, Advanced Experimental Techniques in Powder Metallurgy, pp. 225-252, Plenum Press, New York (1970).
14. R. W. Smithwick and E. L. Fuller, Jr., *Powder Tech.*, 38 165 (1984).

Appendix A. Impurities in MgO Powders

A-1. METALLIC IMPURITIES IN MgO POWDERS AS DETERMINED BY NEUTRON ACTIVATION ANALYSIS

Material	Impurities, ppm (except for *)															
	Na	Ca	Sc	Cr	Mn	Fe	Co	Ni	Zn	As*	Rb	Sr	Zr	Mo*	Sb	Cs
Maglite S	0.80	3200	0.12	9.1	26	240	0.40	<6	14	1700	<3	<40	<40	570	<0.3	<0.2
Morton 90	0.79	4700	0.42	12.5	33	300	0.58	8	8	5500	<3	<50	<50	220	<0.2	<0.2
Maglite A	2.30	<7000	0.14	13.0	42	220	0.35	6	14	1300	<4	<40	<50	920	0.3	<0.2
Baker	0.76	3600	0.32	15.0	58	280	0.57	9	6	4800	<3	<40	<50	140	<0.2	<0.2
Morton 170	0.83	9600	0.52	10.6	135	1170	1.30	7	23	2700	<3	60	<50	290	<0.3	<0.2
Mallinckrodt	1.07	<4000	0.03	9.4	<2	<200	<0.3	<7	10	1300	<4	<80	<50	N.D.	<0.2	<0.2
Martin-Marietta	0.89	3000	0.20	9.0	170	1160	0.27	<5	17	3000	<2	24	<30	N.D.	<0.1	<0.1
Meller	0.76	<3000	0.02	5.4	3.2	100	0.10	2	8	N.D.	<2	<20	<20	N.D.	<0.2	<0.08

Material	Impurities, ppm (except for *)														
	Ba	La	Ce	Nd	Sm	Eu	Tb	Yb	Lu	Hf	Ta	Ir*	Au*	Th	U
Maglite S	<20	1.8	2.4	1.4	0.370	0.07	0.06	0.19	<0.04	<0.20	<0.10	26	600	0.06	1.00
Morton 90	<20	0.3	2.5	<2	0.100	<0.10	<0.1	0.13	0.040	<0.09	<0.20	16	3200	0.19	0.46
Maglite A	<30	2.1	2.2	1.9	0.400	0.10	0.07	0.21	0.027	<0.20	<0.10	16	2600	0.08	1.00
Baker	<20	0.2	1.4	<2	0.088	<0.08	<0.1	0.14	0.014	0.13	<0.20	18	620	0.09	0.46
Morton 170	7	2.3	4.3	<3	0.360	0.08	0.06	0.22	<0.04	0.10	0.05	12	1300	0.35	1.00
Mallinckrodt	9	0.2	0.9	<3	0.004	<0.06	<0.06	<0.20	<0.01	<0.20	<0.10	15	5800	0.11	<0.04
Martin-Marietta	<12	2.6	3.2	1.4	0.220	0.05	0.04	0.14	<0.02	0.06	<0.06	8	800	0.18	0.36
Meller	<8	0.0	<0.5	<1.5	0.006	<0.03	<0.04	<0.05	<0.01	<0.10	<0.07	7	1000	<0.03	0.06

* Values are comparative for a given element and should not be compared to the ppm values for other elements. No standards for the indicated elements were irradiated.
N.D. = Not detected.

A-2. METALLIC IMPURITIES IN MgO POWDERS DETERMINED BY EMISSION SPECTROGRAPHIC ANALYSIS

Material	Impurities, ppm														
	Mg	Ca	Si	Na	Fe	Al	Li	B	Mn	Tl	Cu	Sr	Ag	Zr	Co
Magiite S	Major	400	600	60	150	80	4	350	30	10	6	6	<30	<50	<5
Morton 90	Major	1500	250	10	250	60	6	40	30	60	<2	4	30	<50	<5
Magiite A	Major	400	800	400	100	100	100	6	600	30	10	<2	<30	<50	<5
Baker	Major	400	400	40	150	50	6	40	60	30	4	2	<30	<50	<5
Morton 170	Major	1500	2500	100	1000	1500	6	600	150	40	2	20	1000*	100	<5
Mallinckrodt	Major	10	100	150	30	40	3	<40	<30	<30	<2	<1	30	150	<5
Martin-Marietta	Major	1000	1000	100	1000	400	3	600	200	100	10	5	400	400	<5
Meller	Major	5	60	6	30	150	4	<40	<30	<30	2	<1	50	600*	6

* = Questionable datum.

UNLIMITED DISTRIBUTION

2 Wright Laboratory
Aero Propulsion and Power
Directorate
Att: R. A. Marsh
D. M. Ryan
WL/POOS-2
1950 Fifth St.
Wright-Paterson AFB, OH
45433-7251

3 Argonne National Laboratory
Chemical Technology Div.
Attn: D. Vissers
J. Smaga
T. Kaun
9700 South Cass Ave.
Argonne, IL 604339

2 Army Research Lab
Attn: F. Krieger
A. Goldberg
2800 Powder Mill Road
Adelphi, MD. 20783

1 A. A. Benderly, Consultant
9915 Logan Dr.
Potomac, Maryland 20854

1 Boeing Aerospace
Attn: Chris Johnson
P. O. Box 3999, M/S 82-32
Seattle, WA 98199

5 Eagle-Picher Industries, Inc.
Electronics Div. Couples Dept.
Attn: R. Spencer
F. Smith
J. DeGruson
R. Hudson
J. Wells
P.O. Box 47
Joplin, MO 64802

1 Martin-Marietta
Specialty Components Div.
Attn: W. McCracken
P.O. Box 2908
Largo, FL 34649

1 Naval Ordnance Station
Attn: K. Englander
Code 5123C
Indian Head, MD 20640

2 Naval Surface Warfare Center
Attn: B. Larrick
C. E. Mueller
Silver Springs, MD. 20910

1 Naval Surface Warfare Center
Attn: C. Winchester
Code R33
10901 New Hampshire Ave.
Silver Spring, MD 20903-5000

3 Naval Weapons Center
Attn: M. H. Miles
R. Nolan (Code 3626)
D. Rosenlof (Code 3626)
China Lake, Ca 93555

1 Parker Hannifin
Attn: Arvind Ahluwalia, MS K141
14300 Alton Parkway
Irvine, CA 92718-1814

1 SAFT America
Attn: K. K. Press
107 Beaver Court
Cockeysville, MD 21030

1 Technochem Co.
Attn: Shyam Argade
203A Creekridge Rd.
Greensboro, NC 27406

2 Northrop Grumman
Att: Nick Shuster
Nick Pappadakis
18901 Euclid Ave.
Cleveland, OH 44117

2 DRA Haslar
Materials Dept.
Attn: J. Knight
A. G. Ritchie
Gosport
Room F8, AC Building
Hampshire PO 12 2AG
ENGLAND

1 Leclanche, S.A.
Attn: P. Reutschi
48, Avenue de Grandson
CH-1401 Yverdon-Les-Bain
SWITZERLAND

1 MS0614 D. E. Mitchell, 1522
1 MS0614 A. H. Andazola, 1522
1 MS0614 J. A. Gilbert, 1522
1 MS0614 F. P. Lasky, 1522
1 MS0614 L. M. Moya, 1522
1 MS0614 G. L. Scharrer, 1522
1 MS0614 N. Doddapaneni, 1523
10 MS0614 R. A. Guidotti, 1523
1 MS0614 S. N. Hoier, 1523
1 MS0614 D. Ingersoll, 2523
1 MS0614 G. Nagasubramanian, 1523
1 MS0614 S. N. Hoier, 1523
1 MS0614 D. Ingersoll, 1523
1 MS0614 G. Nagasubramanian, 1523
1 MS0614 F. W. Reinhardt,1523
1 MS9018 Central Technical Files, 8523-2
5 MS0899 Technical Library, 4414
2 MS0619 Review Approval Desk, 12630 for DOE/OSTI